

POLITECNICO DI TORINO

Master of Science in Mechatronic Engineering

Master of Science Thesis

# Modelling and Simulation of the Dynamics of Near Earth Asteroids



POLITECNICO  
DI TORINO

JPL

Jet Propulsion Laboratory  
California Institute of Technology

## Supervisors

Prof. Candido Fabrizio Pirri

Prof. Enrico Canuto

## Candidate

Jorge Alfredo ALVAREZ GUZMAN

Research Mentor  
NASA Jet Propulsion Laboratory

Dr. Marco B. Quadrelli

March 2014



# Acknowledgements

This research was carried out at the Jet Propulsion Laboratory, California Institute of Technology, and was sponsored by the JVSRP Student Program and the National Aeronautics and Space Administration.

Foremost, a special thanks and deep regards to my mentor Dr. Marco B. Quadrelli.

I would also like to express my gratitude to Dr. Abhi Jain, Dr. Jonathan Cameron, Dr. Bob Balaram, Steven Myint, Kalvin Kuo, Hiro Ono and to my fellow interns at JPL for creating a dynamic and intellectually stimulating environment at the DARTS lab, in particular to Mayank for his helpful contributions during my research.

A sincere thanks goes to my italian supervisors, professors Fabrizio Pirri and Enrico Canuto, for giving me the opportunity to have such an edifying experience and for giving me some insight of the field of the research.

I would like to thank Magda, for her support and help during the writing process of this thesis.

Last but not least, I want to dedicate this thesis to my beloved parents and sister, for their words of wisdom and their constant and invaluable support.

# Summary

This research project was aimed to study the main external perturbations that influence the dynamics of Near Earth Asteroids (NEA) and implement their respective models into the DSENDSEduSims simulation platform.

Initially, the background theory of the dynamics of asteroids is presented. Introducing the concept of the two-body problem (Sun-asteroid) and the external perturbations that affect the orbital dynamics and the attitude of the small-body. The *first goal* of this thesis was the implementation of the Solar Radiation Pressure (SRP) model of force and torque, that can be applied to the irregular shape of an asteroid, in order to create a Python[22] function that feeds up the global simulation.

The *second goal* was simulating the dynamics of a specific NEA comparing two different test cases, one for the free response and the other for the forced response of the system. Consequently a study of the effects of the SRP in the behaviour of the state vector, attitude and orbital elements over time was performed. For this purpose an appropriate shape model of the asteroid, divided into finite elements of area, was adopted.

The *third goal* of the research was modelling the shadow effects on asteroids in order to determine individual non-illuminated areas. It may occur in two ways, the first is the self-shadowing effects that appear as a result of the irregular shape of the small-body. The second case occurs when other celestial or non celestial body enter the path of the sunlight creating shadows in the asteroid and therefore introducing small changes in the orbital dynamics.

The *fourth goal* was modelling and developing a Python[22] routine to compute the gravitational potential and gravitational acceleration of planets using spherical harmonics. With the specific objective of including the third-body gravitational perturbations introduced by the aforementioned bodies in a proximity condition. Because of the particular environment of NEA, specific cases for Earth and Moon were further studied.

# Contents

<b>Acknowledgements</b>	III
<b>Summary</b>	IV
<b>1 Introduction</b>	1
1.1 Near Earth Asteroids Overview . . . . .	1
1.2 Hypothesis . . . . .	4
1.3 Simulation outline . . . . .	4
<b>2 Dynamics of Asteroids</b>	7
2.1 Orbital Dynamics . . . . .	7
2.1.1 Reference frames . . . . .	7
2.1.2 Two-body problem . . . . .	10
2.1.3 Classical Orbital Elements . . . . .	13
2.1.4 Free response . . . . .	13
2.1.5 Converting between State Vector and COE . . . . .	17
2.2 Dynamic Equations . . . . .	19
2.3 External Perturbations on Asteroids . . . . .	20
<b>3 Solar Radiation Pressure</b>	23
3.1 Rigid Body Model . . . . .	24
3.2 Finite Elements of Area Model . . . . .	25
3.3 Solar Sail Model . . . . .	26
3.4 Implemented Solar Radiation Pressure Model . . . . .	28
<b>4 Planetary Gravity</b>	29
4.1 Gravitational Potential . . . . .	29
4.1.1 Spherical Harmonics . . . . .	30
4.1.2 Normalised Associated Legendre Functions . . . . .	31
4.2 Gravitational Acceleration Vector . . . . .	31
4.3 Earth Gravitational Model . . . . .	33

4.4	Moon Gravitational Model . . . . .	34
<b>5</b>	<b>Shape Model of Asteroids</b>	<b>37</b>
5.1	NASA Shape Models . . . . .	37
5.2	Gaussian Random Spheres . . . . .	38
<b>6</b>	<b>Tests and Results</b>	<b>43</b>
6.1	Asteroid Dynamics . . . . .	43
6.2	Thin Solar Sail . . . . .	55
6.3	Shadowing Effects . . . . .	58
6.3.1	Theoretical Method . . . . .	58
6.3.2	Implementation . . . . .	58
6.3.3	Shadowing Function . . . . .	59
<b>7</b>	<b>Conclusions and Future Work</b>	<b>63</b>
<b>A</b>	<b>Quaternion definitions</b>	<b>65</b>
A.1	Quaternion representation . . . . .	65
A.2	Quaternion math . . . . .	66
A.2.1	Norm . . . . .	66
A.2.2	Normalization . . . . .	66
A.2.3	Conjugate . . . . .	66
A.2.4	Addition . . . . .	67
A.2.5	Multiplication . . . . .	67

# List of Tables

1.1	Near Earth Objects Classification. $q$ , $Q$ , $P$ and $a$ represent the perihelion radius, aphelion radius, orbit period, and semi-major axis respectively. [22]	4
1.2	ExternalForce Module Description	6
2.1	Definition of the Classical Orbital Elements	14
2.2	Type of conic section	15
2.3	Probabilistic error modelling of environmental forces on the Galileo spacecraft [N] [12]	21
2.4	Probabilistic error modelling of secular precessional torques on the Galileo spacecraft [Nm] [12]	22
4.1	Variation of gravitational potential and gravitational acceleration of the Earth with the degree	34
4.2	Variation of Moon's gravitational potential and gravitational acceleration with the degree	35
5.1	Gaussian random sphere (1620) Geographos parameters	41
6.1	Initial orbital elements of asteroid (1620) Geographos	43
6.2	Initial state vector of the CoM of asteroid (1620) Geographos	44
6.3	Initial attitude of asteroid (1620) Geographos referred to the body frame	44
6.4	Body properties of asteroid (1620) Geographos	44

# List of Figures

1.1	Asteroid and comet locations in their heliocentric orbits [Credit: P. Chodas, NASA/JPL-Caltech]	2
1.2	Near Earth Asteroid (1620) Geographos Orbit [Courtesy NASA/JPL-Caltech]	3
1.3	Asteroid Distribution in the Inner Solar System [Credit: Alan Chamberlin, NASA/JPL-Caltech]	3
2.1	Coordinate reference frames [Courtesy NASA/JPL-Caltech]	8
2.2	Body-fixed reference frame [Courtesy Enrico Canuto]	9
2.3	Two-body problem geometry [Courtesy Enrico Canuto]	10
2.4	Classical Orbital Elements [11]	13
2.5	Eccentric and Mean anomaly [1]	16
2.6	"Bell Curve" Standard Normal (Gaussian) Distribution [20]	22
3.1	Components of Reflection [18]	23
3.2	Diagram of vectors for the non-ideal solar sail[21]	26
5.1	(1620) Geographos Radar-based Polyhedron Shape Model	38
5.2	Polyhedron-based model of asteroid (1620) Geographos	41
6.1	Orbital trajectory of the centre-of-mass of asteroid (1620) Geographos	45
6.2	(1620) Geographos CoM Position [AU] vs Simulation Time [yr]	46
6.3	(1620) Geographos CoM Velocity [ $\frac{m}{s}$ ] vs Simulation Time [yr]	47
6.4	(1620) Geographos CoM Acceleration [ $\frac{m}{s^2}$ ] vs Simulation Time [yr]	48
6.5	(1620) Geographos body-frame quaternion vs Simulation Time [yr]	49
6.6	(1620) Geographos Orbital Elements vs Simulation Time [yr]	50
6.7	(1620) Geographos Perturbation in Orbital Elements vs Simulation Time [yr]	51
6.8	(1620) Geographos Gravitational Force [N] vs Simulation Time [yr]	52
6.9	(1620) Geographos SRP Force [N] vs Simulation Time [yr]	53
6.10	(1620) Geographos SRP Torque [Nm] vs Simulation Time [yr]	54
6.11	Solar sail Finite Element Model	55
6.12	Force exerted on a 100 x 100 $m^2$ square solar sail at 1 AU	56
6.13	Force Error [N] vs Incident Angle [deg]	57
6.14	Render showing the ray grid collision test	58

6.15	Render showing the shadowing function on asteroid (1620) Geographos	60
6.16	Render showing the shadowing function on a primitive object (Sphere)	61
6.17	Illuminated solar sail with collision points	61

# Chapter 1

## Introduction

This chapter is intended to provide the reader with both a basic overview of the subject of this dissertation and a familiarisation with the motivation of the study, simulation environment and developed routines.

### 1.1 Near Earth Asteroids Overview

Asteroids are small bodies in the *solar system* that orbit the Sun, which means that their orbits are heliocentric as is the case for all of the planets in the solar system. They are composed of rock and metals and have irregular shapes due to the fact that they are not as massive as planets, as a result of this they may rotate in peculiar ways. They are mainly located in the *main belt* (between the orbits of Mars and Jupiter) as can be seen in Figure 1.1. For a more specific look at their distribution in the inner solar system please see Figure 1.3, in which they are classified depending on the eccentricity and semi-major axis of their elliptical orbits. These parameters indicate how much they deviate from a circular orbit and what is the distance from the centre to the farthest point of the orbit respectively (Orbital Elements will be further explained in Chapter 2). Nevertheless, the proximity of some of these bodies with the planet Earth prompt to the definition of Near Earth Asteroids.

Near Earth Asteroids (NEA) are asteroids whose heliocentric orbits cross the Earth's orbit and its closest approach to the Sun is below 1.3 AU<sup>1</sup>, as is displayed in the orbit of asteroid (1620) Geographos in Figure 1.2. Their study is of great importance on the grounds that some of them may collide with Earth. The probability of an asteroid smashing into Earth and causing significant damage is very remote, but the devastating consequences of such an impact motivates the study of NEA to understand their compositions, structures, sizes, and future trajectories[28]. In other cases their proximity is translated into a feasible way of understanding the formation of our solar system, since asteroids are considered as part of the remains

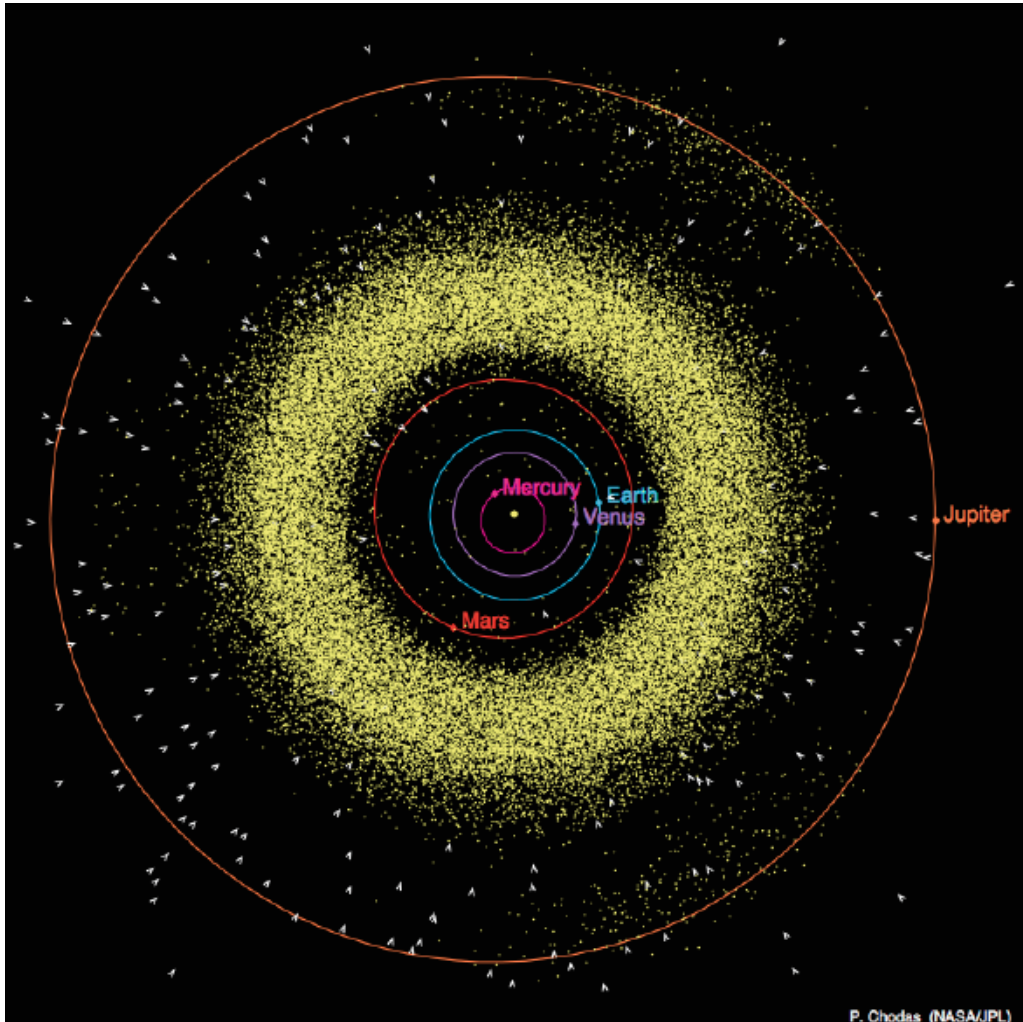


**Figure 1.1:** Asteroid and comet locations in their heliocentric orbits [Credit: P. Chodas, NASA/JPL-Caltech]

from its formation process and their composition has not changed in billions of years.

They are usually classified, depending on their heliocentric orbits, as a subclass of the bigger group of Near Earth Objects (NEO) that contain also the Near Earth Comets (NEC) as reported in Table 1.1. They differ with the latter because of their formation, composition, orbit and stability of the surface.

---

<sup>1</sup>1 AU = 149,597,870.700 km (mean distance between the Earth and the Sun)[28].

<sup>2</sup>yr is the adopted symbol for years.

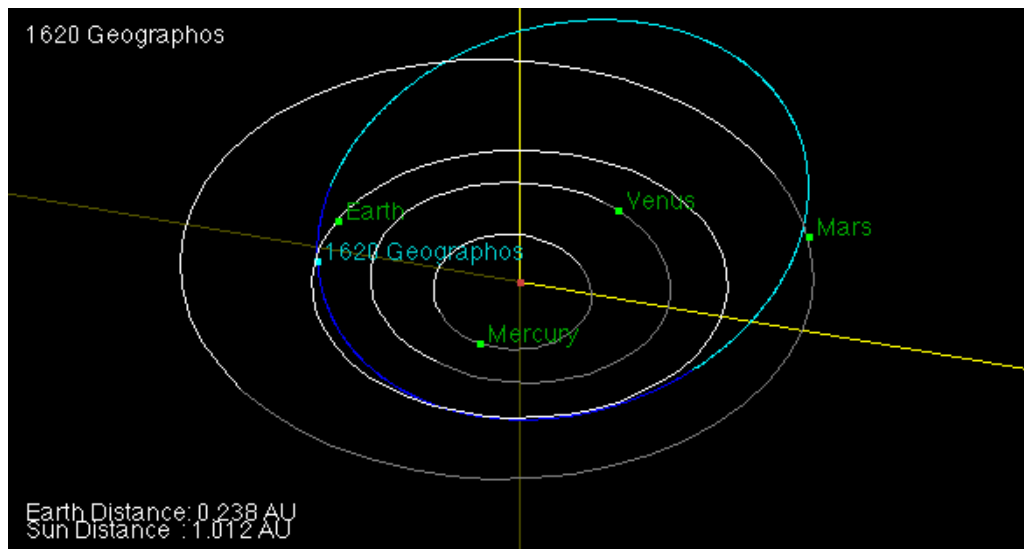


**Figure 1.2:** Near Earth Asteroid (1620) Geographos Orbit [Courtesy NASA/JPL-Caltech]

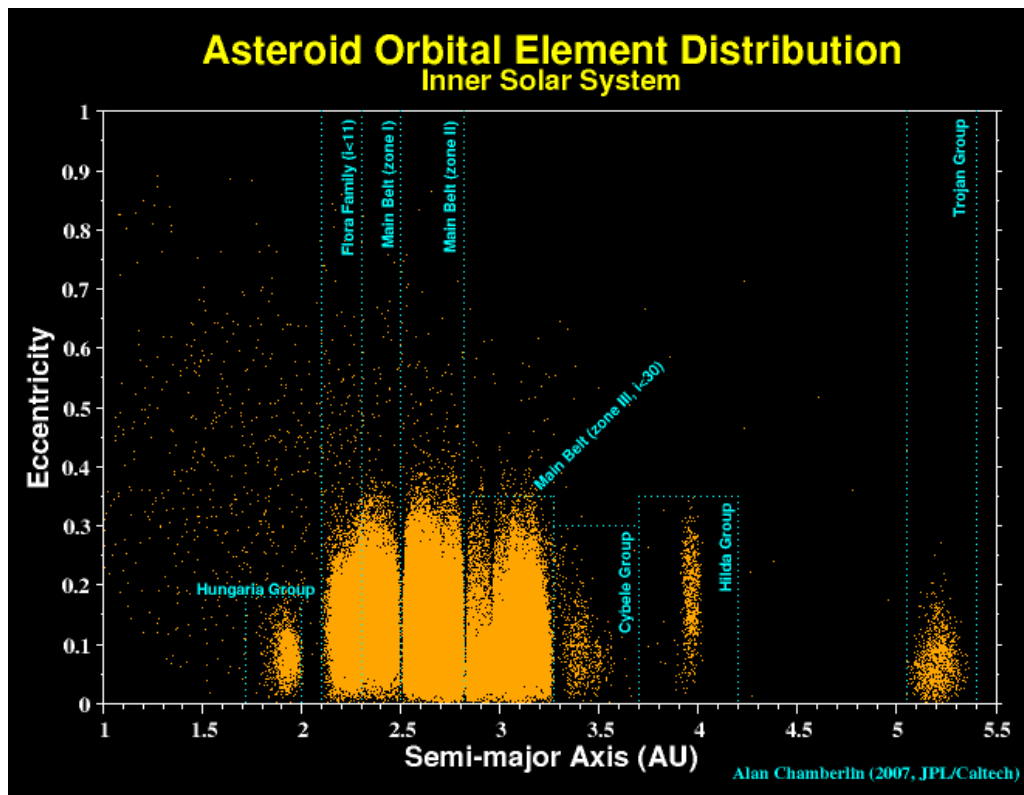


**Figure 1.3:** Asteroid Distribution in the Inner Solar System [Credit: Alan Chamberlin, NASA/JPL-Caltech]

Group	Description	Definition
NEC	Near Earth Comets	$q < 1.3 \text{ [AU]}$ $P < 200 \text{ [yr}^2]$
NEA	Near Earth Asteroids	$q < 1.3 \text{ [AU]}$
Atiras	NEAs whose orbits are contained entirely with the orbit of the Earth (named after asteroid 163693 Atira).	$a < 1.0 \text{ [AU]}$ $Q < 0.983 \text{ [AU]}$
Atens	Earth-crossing NEAs with semi-major axes smaller than Earth's (named after asteroid 2062 Aten).	$a > 1.0 \text{ [AU]}$ $Q > 0.983 \text{ [AU]}$
Apollos	Earth-crossing NEAs with semi-major axes larger than Earth's (named after asteroid 1862 Apollo).	$a > 1.0 \text{ [AU]}$ $1.017 < q < 1.3 \text{ [AU]}$
Amors	Earth-approaching NEAs with orbits exterior to Earth's but interior to Mars' (named after asteroid 1221 Amor).	$a > 1.0 \text{ [AU]}$ $q < 1.017 \text{ [AU]}$
PHAs	Potentially Hazardous Asteroids: NEAs whose Minimum Orbit Intersection Distance (MOID) with the Earth is 0.05 AU or less and whose absolute magnitude ( $H$ ) is 22.0 or brighter.	$MOID \leq 0.05 \text{ [AU]}$ $H \leq 22.0$

**Table 1.1:** Near Earth Objects Classification.  $q$ ,  $Q$ ,  $P$  and  $a$  represent the perihelion radius, aphelion radius, orbit period, and semi-major axis respectively. [22]

## 1.2 Hypothesis

The aim of this thesis is to give the reader the sufficient insight into the research developed, in which the global objective was to implement a model within the simulating platform for each of the considerable *external perturbations* (forces and torques) acting on an asteroid. The starting hypothesis is that the dynamics of NEA, other than the gravitational force of the Sun, are predominantly affected by the Solar Radiation Pressure (SRP) and the gravitational force exerted by the planet Earth and the Moon.

## 1.3 Simulation outline

The simulation environment in which the problem is developed is the DSENDSEdu platform. DSENDSEdu is a high-fidelity simulator for planetary and small-body<sup>3</sup>dynamics

developed at the Jet Propulsion Laboratory (JPL). In Figure 1.2 a description of the developed ExternalForce module is presented. It contains the principal scripts, routines and functions necessary for the simulation of the theory that will be described in the following Chapters. All of the scripts were builded up using Python[26] as the programming language.

---

<sup>3</sup>Small-body, also known as small solar system body (SSSB) is an object in the solar system that is neither a planet, nor a dwarf planet, nor a satellite.

---

Folder	Description
OrbitalParameters	Folder containing Python functions to transform from Classical Orbital Elements to state vector ( <code>COE2rv.py</code> ) or viceversa ( <code>rv2COE.py</code> ). <code>PerturbationCOE.py</code> is a function to calculate the perturbation in the COE.
SolarPressure	Folder containing all the scripts needed to compute the Solar Radiation Pressure. <code>SolarPressure.py</code> , <code>SolarPressureFEM.py</code> and <code>SolarPressureSolarSail.py</code> contain the models of tested versions of the SRP.
ShapeModels	Folder containing the shape models of asteroids as they were adapted from the source files found at <a href="http://pds.nasa.gov/">http://pds.nasa.gov/</a> . Including the shape model of asteroid (1620) Geographos.
Shadowing	Folder containing all the scripts that compute the shadowing effect. Examples for asteroid (1620) Geographos, an ideal Solar Sail and a primitive object (sphere) have been written. <code>test_graphical.py</code> displays the rendered image of the asteroid with the collisions and the shadowed areas. <code>test_nongraphical.py</code> prints the collision positions.
PlanetaryGravity	Folder containing scripts that calculate the gravitational potential and acceleration of the Earth and the Moon using spherical harmonics. Data input from the Earth Gravitational Model (EGM2008) and Lunar Prospector mission (LP150) has been used. <code>LegendreFunctions.py</code> is a function that calculated the normalised associated Legendre polynomials needed to compute the spherical harmonics. <code>sphericalharmonics.py</code> is a recursive function that calculates the gravitational potential and acceleration.
test	Folder containing a diversity of test performed using SRP. <code>test_1620Geographos</code> implements the orbital dynamics of asteroid (1620) Geographos and measures the effect of SRP. <code>test_SolarSail</code> implements a validating test case for the SRP model of a Solar Sail.

---

**Table 1.2:** ExternalForce Module Description

# Chapter 2

## Dynamics of Asteroids

In this chapter the reader will be introduced to the framework of the dynamics of asteroids, as they constitute the base for this thesis project. Initially, an outline of the orbital dynamics of the asteroid will be provided, delineating the main reference frames needed in our particular problem, along with the parameters that characterise the gravitational motion between the celestial bodies. Afterwards, the dynamic equations that govern the system will be reported, giving significant importance to the attitude dynamics of the asteroid. Finally, there will be a description of the principal external perturbations acting on the small-body, making an assessment on the focus of our study in the following chapters.

### 2.1 Orbital Dynamics

The orbital dynamics of the Center of Mass (CoM) of an asteroid can be seen in two parts. First, the free response of the system is characterised by the Sun's gravitational force. It defines the motion of the asteroid, an elliptical trajectory with the Sun in one of the focus. Second, other external forces and torques will be seen as perturbations, such as the Solar Radiation Pressure (SRP) and the Planetary Gravity. The ensemble of these perturbations define the forced response of the system.

#### 2.1.1 Reference frames

In order to characterise the motion of the asteroid in space, first we have to define the appropriate reference frames, and for each of them its three orthogonal unit vectors. A reference frame is defined by a reference plane, and a reference direction that is located in the aforementioned. In Figure 2.1 two reference planes are shown in the *Celestial Sphere* (sphere with infinite radius centered on the Sun). As will be

stated next:

- The first one is the *Ecliptic*, a quasi-inertial plane defined by the apparent motion of the Sun during the year. Its marginal change is due to lunar and solar precession, nutation and other planetary perturbations.
- The second one is the *Celestial Equator*, a non-inertial plane defined by the projection of Earth's equator. It has an obliquity ( $\epsilon$ ) of 23.44 degrees with respect to the former.

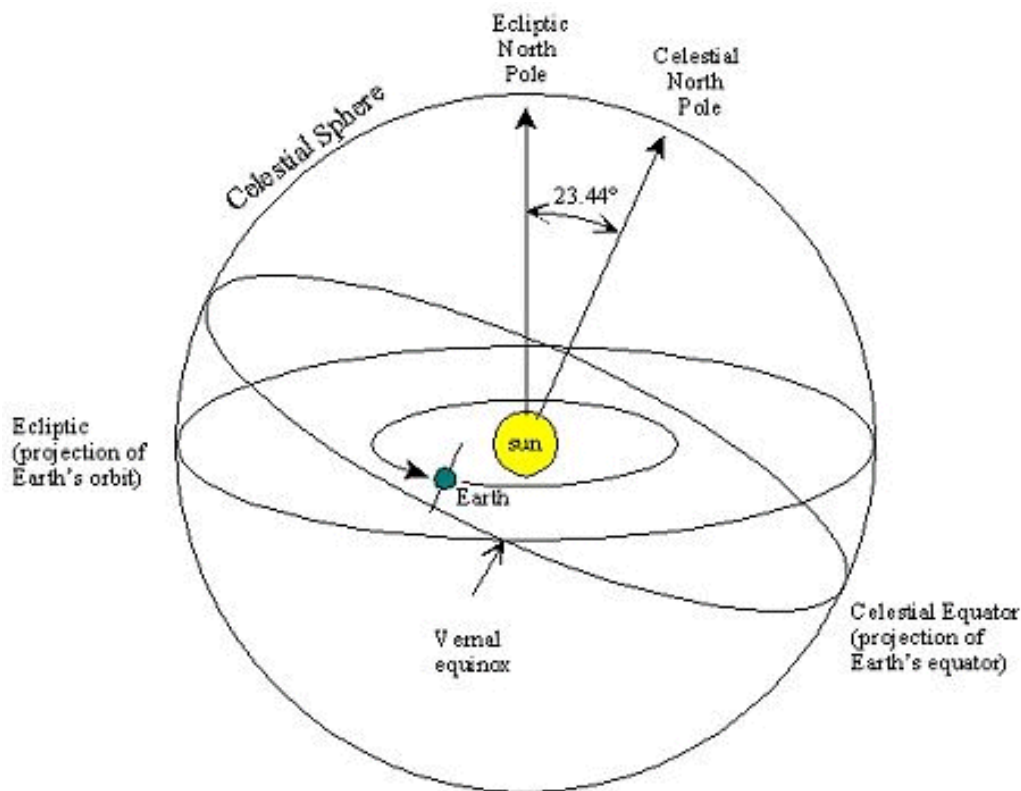


**Figure 2.1:** Coordinate reference frames [Courtesy NASA/JPL-Caltech]

A standard Ecliptic plane is often used at the *J2000.0* epoch on January 1, 2000, 11:58:55.816 UTC. The reference direction is the *Vernal equinox* ( $\gamma$ ), which is the point on the Celestial Sphere at the intersection of the Celestial Equator and the Ecliptic, where the Sun crosses the Equator from south to north in its apparent annual motion along the Ecliptic[3]. This reference frame (otherwise called *International Celestial Reference Frame*) is considered to be inertial, and it is written as:

$$R_J = \{O, \hat{i}_J, \hat{j}_J, \hat{k}_J\}$$

Where the origin  $O$  is the CoM of the solar system. The plane formed by  $\{O, \hat{i}_J, \hat{j}_J\}$  is aligned with the Equator (*Mean Equator*), and  $\hat{i}_J$  points to the Vernal equinox (*Mean equinox*). The Julian J2000  $R_J$  reference frame is used on the DSENDSEdu platform.

The other important reference frames to be defined are:

- The *body-fixed reference frame (body-frame)*, is defined by an origin and two points that define the pole and the orthogonal plane. Can be formalised as follows:

$$R_b = \{C, \hat{b}_1, \hat{b}_2, \hat{b}_3\}$$

Where, as displayed in Figure 2.2,  $C$  is the CoM of the rigid body (asteroid in our case).  $\hat{b}_3 = \frac{\overline{CP_1}}{|\overline{CP_1}|}$  is unit vector in the direction of the pole.  $\hat{b}_1 = \frac{\overline{CP_2}}{|\overline{CP_2}|}$  is the unit vector defined by a point  $P_2$  that lies in the orthogonal plane ( $\Pi$ ) to  $\hat{b}_3$ . And  $\hat{b}_2 = \hat{b}_3 \times \hat{b}_1$  is simply constructed to be orthogonal to both  $\hat{b}_3$  and  $\hat{b}_1$ .

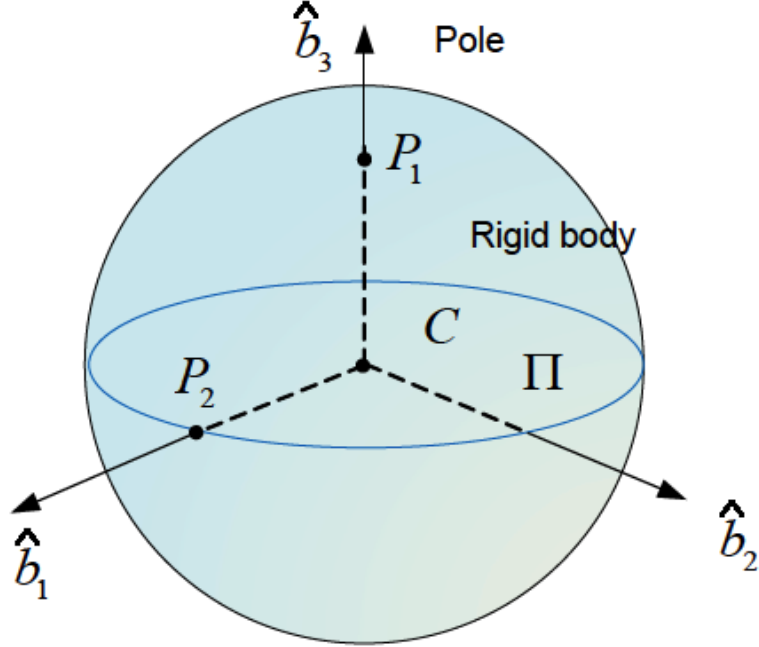


**Figure 2.2:** Body-fixed reference frame [Courtesy Enrico Canuto]

- The *Local Vertical Local Horizontal (LVLH)* reference frame, has its origin in the CoM  $C$  of the body. A modified heliocentric version of the one found in [3]. Written thus and so:

$$R_l = \{C, \hat{l}_1, \hat{l}_2, \hat{l}_3\}$$

Where  $\hat{l}_3$  lies along the heliocentric radius vector to the asteroid, and is positive towards the centre of the Sun.  $\hat{l}_1$  lies in the vertical orbital plane, perpendicular to  $\hat{l}_3$  and positive in the direction of the asteroid motion.  $\hat{l}_2 = \hat{l}_3 \times \hat{l}_1$  completes the right handed orthogonal set of unit vectors, similar to the body-frame case.

- The *Perifocal Reference Frame (PQW)*, quasi-inertial Sun-centered reference frame given by:

$$R_{PQW} = \{O, \hat{p}, \hat{q}, \hat{w}\}$$

Where its origin  $O$  as previously said is the CoM of the Sun.  $\hat{p} = \frac{\underline{e}}{e}$  is the unit vector in the direction of the perihelion of the elliptical orbit (given by the *eccentricity vector*  $\underline{e}$ ).  $\hat{w} = \frac{\underline{h}}{h}$  is the unit vector given by the *angular momentum vector* ( $\underline{h}$ ). And  $\hat{q} = \hat{w} \times \hat{p}$  completes the right handed orthogonal set of unit vectors.

### 2.1.2 Two-body problem

The two-body problem describes the motion of two bodies in mutual gravitational attraction. These two bodies may have an arbitrarily shape and mass, but for the scope of this thesis is restricted to study the dynamics of an asteroid  $\mathbf{m}_1$ , about a massive and nearly spherically-symmetric body (Sun),  $\mathbf{m}_0$ .

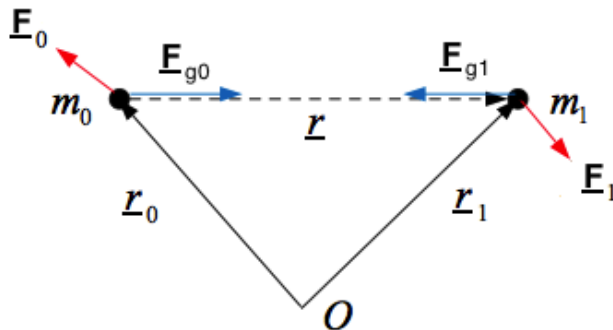


**Figure 2.3:** Two-body problem geometry [Courtesy Enrico Canuto]

In Figure 2.3 the problem is illustrated. The position and velocity are defined in an inertial frame  $R\{O, \hat{i}_1, \hat{i}_2, \hat{i}_3\}$ , therefore the state vector of the Sun and asteroid are  $\{\underline{r}_0, \underline{v}_0\}$  and  $\{\underline{r}_1, \underline{v}_1\}$  respectively.

Newton's law of universal gravitation states that any two bodies attract one another with a force proportional to the product of their masses and inversely proportional to the square of the distance between. Defining the relative position between them,  $\underline{r} = \underline{r}_1 - \underline{r}_0$ , its magnitude,  $r = |\underline{r}|$ , and the universal gravity constant,  $G = 6.67259 \cdot 10^{-11} [\frac{m^3}{kg s^2}]$  [23], the mathematical equations in our case are defined as:

$$\underline{F}_{g0} = \frac{Gm_0m_1}{r^2} \frac{\underline{r}}{r} \quad (2.1)$$

$$\underline{F}_{g1} = -\frac{Gm_0m_1}{r^2} \frac{\underline{r}}{r} \quad (2.2)$$

Applying Newton's second law, using the gravitational forces in Equations 2.1 and 2.2, and with the forces  $\underline{F}_0$  and  $\underline{F}_1$  being the external perturbations, we describe the system in a set of six equations per body. Where the state variables,  $\{\underline{r}_0, \underline{v}_0\}$  and  $\{\underline{r}_1, \underline{v}_1\}$ , are written as follows:

$$\dot{\underline{r}}_0 = \underline{v}_0 \quad (2.3)$$

$$\dot{\underline{v}}_0 = \frac{Gm_0m_1}{m_0r^3} \underline{r} + \frac{\underline{F}_0}{m_0} \quad (2.4)$$

$$\dot{\underline{r}}_1 = \underline{v}_1 \quad (2.5)$$

$$\dot{\underline{v}}_1 = -\frac{Gm_0m_1}{m_1r^3} \underline{r} + \frac{\underline{F}_1}{m_1} \quad (2.6)$$

With initial conditions:

$$\underline{r}_0(0) = r_{00}, \underline{v}_0(0) = v_{00}, \underline{r}_1(0) = r_{10}, \underline{v}_1(0) = v_{10}$$

Making a linear change of variables employing the relative motion between the two bodies,  $\underline{r} = \underline{r}_1 - \underline{r}_0$  and  $\underline{v} = \underline{v}_1 - \underline{v}_0$ , we find a new set of six equations with state variables  $\{\underline{r}, \underline{v}\}$ , in this manner:

$$\dot{\underline{r}} = \dot{\underline{r}}_1 - \dot{\underline{r}}_0 = \underline{v}_1 - \underline{v}_0 = \underline{v} \quad (2.7)$$

$$\dot{\underline{v}} = \dot{\underline{v}}_1 - \dot{\underline{v}}_0 = -\frac{G(m_0 + m_1)}{r^3} \underline{r} + \frac{\underline{F}_1}{m_1} - \frac{\underline{F}_0}{m_0} \quad (2.8)$$

It is convenient to find the state vector of the CoM. Performing another linear change of variables, we define the position and velocity of the CoM in this way:

$$\underline{r}_{CoM} = \frac{m_0}{m_0 + m_1} \underline{r}_0 + \frac{m_1}{m_0 + m_1} \underline{r}_1 \quad (2.9)$$

$$\underline{v}_{CoM} = \frac{m_0}{m_0 + m_1} \underline{v}_0 + \frac{m_1}{m_0 + m_1} \underline{v}_1 \quad (2.10)$$

Using Equations 2.3, 2.4, 2.5, 2.6 and Equations 2.9, 2.10 the set of equations for the state vector of the CoM is presented, thus and thus:

$$\dot{\underline{r}}_{CoM} = \frac{m_0}{m_0 + m_1} \dot{\underline{r}}_0 + \frac{m_1}{m_0 + m_1} \dot{\underline{r}}_1 = \underline{v}_{CoM} \quad (2.11)$$

$$\dot{\underline{v}}_{CoM} = \frac{m_0}{m_0 + m_1} \dot{\underline{v}}_0 + \frac{m_1}{m_0 + m_1} \dot{\underline{v}}_1 = \frac{\underline{F}_0 + \underline{F}_1}{m_0 + m_1} \quad (2.12)$$

From Equations 2.11 and 2.12, it is confirmed that the gravitational force is internal to the system since the set of equations of the CoM does not depend on it, but depends only on the external forces applied to the bodies.

Moreover, with the mass of the asteroid being negligible compared to the mass of the Sun ( $m_0 \gg m_1$ ) and assuming finite external forces, Equations 2.8 and 2.12 simplify, the new set of equations therefore is rewritten as follows:

$$\dot{\underline{r}} = \underline{v} \quad (2.13)$$

$$\dot{\underline{v}} \approx -\frac{Gm_0}{r^3} \underline{r} + \frac{\underline{F}_1}{m_1} = -\frac{\mu}{r^3} \underline{r} + \frac{\underline{F}_1}{m_1} \quad (2.14)$$

$$\dot{\underline{r}}_{CoM} = \underline{v}_{CoM} \quad (2.15)$$

$$\dot{\underline{v}}_{CoM} \approx 0 \quad (2.16)$$

With initial conditions:

$$\underline{r}(0) = r_0, \underline{v}(0) = v_0, \underline{r}_{CoM}(0) = r_{CoM0}, \underline{v}_{CoM}(0) = v_{CoM0}$$

Where  $\mu = Gm_0 = 1.32712440018 \cdot 10^{20} [\frac{m^3}{s^2}]$  [23] is the standard gravitational parameter of the Sun in our specific case. Since the acceleration of the CoM approximates to zero (Equation 2.16),  $r_{CoM}$  may be selected as the centre of an inertial frame of reference. Confirming our statement that the CoM of the solar system is selected as the origin of the Julian J2000 reference frame. In particular since the mass of the asteroid is negligible compared to that of the Sun, the latter can be selected as the origin of the reference frame.

### 2.1.3 Classical Orbital Elements

In order to describe the asteroid orbital dynamics it is necessary first to characterise the Classical Orbital Elements (COE) that are required to outline a specific orbit. These elements are considered in a two-body classical system, one of the bodies being the Sun and the other an asteroid orbiting the first one. In general it takes six parameters to uniquely define an orbit and its relative state vector. The six Keplerian classical elements used to describe the motion of a celestial body are reported in Table 2.1. In Figure 2.4 the orbit of the Celestial body is displayed with its respective orbital elements. In this case, as stated in Section 2.1.1, the plane of reference is the standard J2000 Ecliptic plane, and the reference direction is the Vernal Equinox.

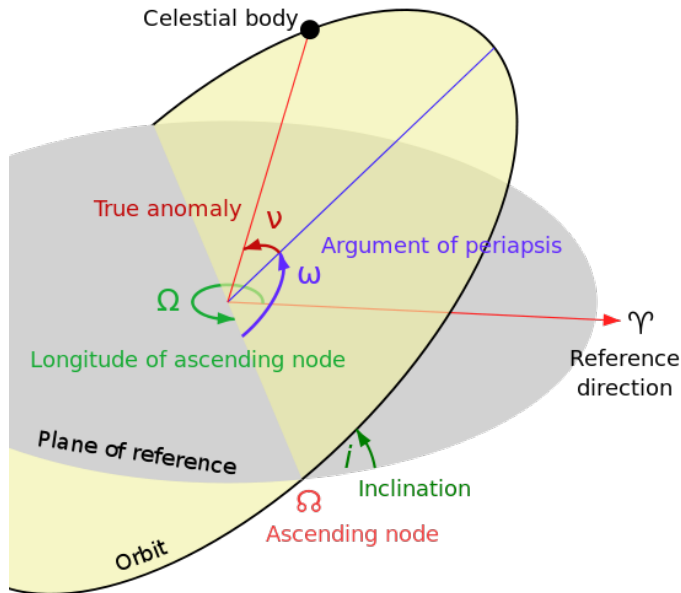


**Figure 2.4:** Classical Orbital Elements [11]

### 2.1.4 Free response

In order to obtain the free response behaviour of the system, Equations 2.13 and 2.14 are simplified by setting the input from the external forces to zero. The following equations are obtained:

$$\dot{\underline{r}} = \underline{v}, \quad \underline{r}(0) = \underline{r}_0 \quad (2.17)$$

$$\dot{\underline{v}} = -\frac{\mu}{r^3} \underline{r}, \quad \underline{v}(0) = \underline{v}_0 \quad (2.18)$$

Parameter	Description
Semimajor-axis ( $\mathbf{a}$ )	Defines the size of the orbit
Eccentricity ( $\mathbf{e}$ )	Defines the shape of the orbit
Inclination ( $\mathbf{i}$ )	Defines the inclination of the orbit with respect to the reference (ecliptic) plane measured from the ascending node
Argument of the perihelion ( $\omega$ )	Defines the orientation of the orbit in the orbital plane, as an angle measured from the ascending node to the perihelion
Longitude of the Ascending Node ( $\Omega$ )	Defines the location of the ascending and descending orbit locations with respect to the reference (ecliptic) plane
True Anomaly ( $\nu$ )	Defines where the body is within the orbit with respect to perihelion

**Table 2.1:** Definition of the Classical Orbital Elements

It is convenient then to define the angular momentum vector,  $\underline{h}$ , of the asteroid with respect to the Sun, and its time derivative as follow:

$$\underline{h} = \underline{r} \times \underline{v} \quad (2.19)$$

$$\dot{\underline{h}} = \underline{r} \times \dot{\underline{v}} + \dot{\underline{r}} \times \underline{v} = 0 \quad (2.20)$$

Since the time derivative of the angular momentum vector in Equation 2.20 is zero due to cross-product properties, the orbital plane can be considered as an inertial frame of reference. Now we consider the following equation:

$$\begin{aligned} \dot{\underline{v}} \times \underline{h} - \dot{\underline{v}} \times \underline{h} &= 0 \\ \dot{\underline{v}} \times \underline{h} + \frac{\mu}{r^3} \underline{r} \times \underline{h} &= 0 \\ \frac{d}{dt} \left( \underline{v} \times \underline{h} - \mu \frac{\underline{r}}{r} \right) &= 0 \\ \underline{v} \times \underline{h} - \mu \frac{\underline{r}}{r} &= \mu \underline{e} \end{aligned} \quad (2.21)$$

The orbit of the asteroid describes an elliptical trajectory in which the Sun is one of the focus. In Equation 2.21, the eccentricity vector  $\underline{e}$  is defined. This vector

is constant, lies on the orbital plane and points out to the perihelion.

Multiplying both sides of Equation 2.21 by  $\underline{r}^T$  we may find:

$$\underline{r}^T(\underline{v} \times \underline{h}) - \frac{\mu}{r}\underline{r}^T\underline{r} = \mu\underline{r}^T\underline{e}$$

Applying mixed properties:

$$h^2 - \mu r(t) = \mu r(t)e \cos(\nu(t))$$

Finally finding an expression for the radius of the orbit as follows:

$$r(t) = \frac{p}{1 + e \cos(\nu(t))} \quad (2.22)$$

Equation 2.22 is in fact the *orbit equation*, otherwise named *trajectory equation*. Where  $p = \frac{h^2}{\mu}$  is called *parameter*.  $e = |\underline{e}|$ , as seen in Table 2.1 is the eccentricity of the orbit.  $\nu(t)$ , the angle between  $\underline{r}$  and  $\underline{e}$ , is the true anomaly, also reported in Table 2.1. And  $h = |\underline{h}|$  is the magnitude of the angular momentum vector. Furthermore this equation describes the shape and size of the orbit, indicating that all asteroid orbits are conic sections: ellipses, circles, parabolas and hyperbolas.

Conic Section	Eccentricity
Circle	$e = 0$
Ellipse	$0 < e < 1$
Parabola	$e = 1$
Hyperbola	$e > 1$

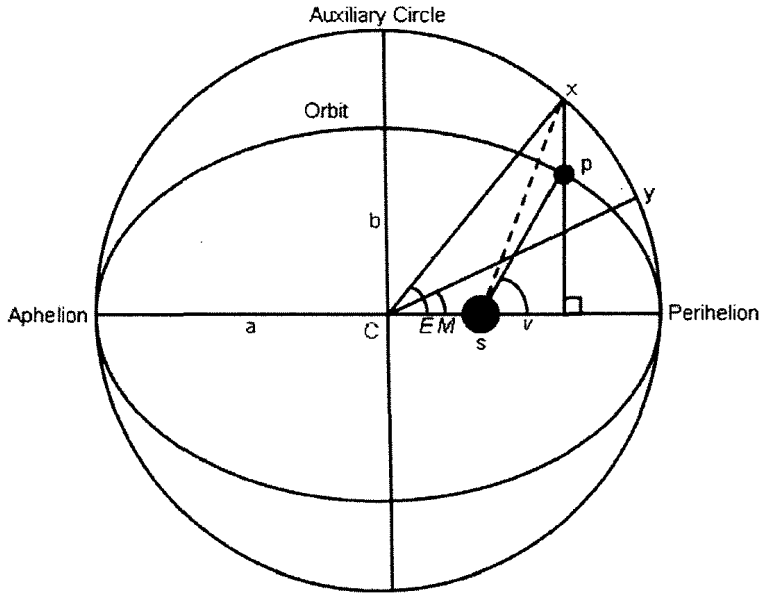
**Table 2.2:** Type of conic section

Table 2.2 shows the different type of conic sections, and therefore all of the possible orbits that the asteroid may describe depending on the eccentricity.

Normally the motion of the asteroid within the orbit is described by the true anomaly ( $\nu$ ), but it can be replaced by the *eccentric anomaly* ( $E$ ), which is the angular distance between the perihelion and the projection of the position of the elliptical orbit into its *auxiliary circle* of radius  $a$ , measured from the centre of the orbit (as seen in Figure 2.5). Now we present the differential equation that defines this motion, a modified version of Kepler's equation, like this:

$$\dot{E}(t)(1 - e \cos(E(t))) = \omega_0, \quad E(0) = 0 \quad (2.23)$$

With *mean angular rate* and *mean orbital period*, respectively:



**Figure 2.5:** Eccentric and Mean anomaly [1]

$$\omega_0 = \sqrt{\frac{\mu}{a^3}} \quad [\text{rad/s}]$$

$$p_0 = \frac{2\pi}{\omega_0} \quad [\text{s}]$$

The mean angular rate is the constant angular rate that the asteroid would have in a circular orbit ( $e = 0$ ), and the mean angular period would be its period in such case. Solving Equation 2.23 we find the *Free Response* equation:

$$E(t) = e \sin(E(t)) + \omega_0(t - t_0), \quad t \geq t_0 \quad (2.24)$$

$$r(t) = a(1 - e \cos(E(t))) \quad (2.25)$$

The linear part of Equation 2.24 is called *mean anomaly*,  $M(t) = \omega_0(t - t_0)$ . In the particular case of a circular orbit, since we have zero eccentricity ( $e = 0$ ), Equation 2.24 and Equation 2.25 simplify, and therefore we obtain:

$$E(t) = \omega_0(t - t_0), \quad t \geq t_0 \quad (2.26)$$

$$r(t) = a \quad (2.27)$$

As expected the radius of the orbit is equivalent to  $a$ , and in this case the eccentric anomaly and the mean anomaly are identical.

### 2.1.5 Converting between State Vector and COE

From the COE it is possible to calculate the orbital state vector. The state vector of position ( $\underline{r}$ ) and velocity ( $\underline{v}$ ), previously employed in Equations 2.13 and 2.14, uniquely determine the trajectory of the orbit of an asteroid. They may be expressed in cartesian coordinates with respect to the inertial frame, as follows:

$$\underline{r} = x_1 \hat{i} + x_2 \hat{j} + x_3 \hat{k}$$

$$\underline{v} = v_1 \hat{i} + v_2 \hat{j} + v_3 \hat{k}$$

A couple of algorithms to transform from COE to state vector and vice versa were implemented as Python functions. Both of them are of vital importance during our simulations. The state vector is needed to compute the orbital dynamics, and the COE allow us to study the orbital dynamics and its variation over time.

- *State Vector to COE Algorithm*

The algorithm to transform from the State Vector to COE found in [25] is presented:

$$(a, e, i, \Omega, \omega, \nu) = rv2COE(\underline{r}, \underline{v})$$

$$\underline{h} = \underline{r} \times \underline{v}$$

$$\underline{n} = \hat{k} \times \underline{h}$$

$$e = \frac{\left(v^2 - \frac{\mu}{r}\right) \underline{r} - (\underline{r} \cdot \underline{v}) \underline{v}}{\mu}$$

$$\xi = \frac{v^2}{2} - \frac{\mu}{r}$$

If  $e \neq 1.0$  then:

$$a = -\frac{\mu}{2\xi}$$

$$p = (1 - e^2)$$

else:

$$p = \frac{h^2}{\mu} \quad \text{and} \quad a = \infty$$

$$\cos(i) = \frac{h_k}{|\underline{h}|}$$

$$\cos(\Omega) = \frac{n_i}{|\underline{n}|} \quad \text{if } (n_j < 0) \text{ then } \Omega = 360^\circ - \Omega$$

$$\cos(\omega) = \frac{\underline{n} \cdot \underline{e}}{|\underline{n}||\underline{e}|} \quad \text{if } (e_k < 0) \text{ then } \omega = 360^\circ - \omega$$

$$\cos(\nu) = \frac{\underline{e} \cdot \underline{r}}{|\underline{e}||\underline{r}|} \quad \text{if } (\underline{r} \cdot \underline{v} < 0) \text{ then } \nu = 360^\circ - \nu$$

- COE to State Vector Algorithm

The algorithm to transform from COE to the State Vector found in [25] is presented:

$$(\underline{r}, \underline{v}) = COE2rv(a, e, i, \Omega, \omega, \nu)$$

$$\underline{r}_{PQW} = \left[ \frac{p \cos(\nu)}{1 + e \cos(\nu)}, \frac{p \sin(\nu)}{1 + e \cos(\nu)}, 0 \right]$$

$$\underline{v}_{PQW} = \left[ -\sqrt{\frac{\mu}{p}} \sin(\nu), \frac{\mu}{p}(e + \cos(\nu)), 0 \right]$$

$$\underline{r} = [PQW2IJK] \underline{r}_{PQW}$$

$$\underline{v} = [PQW2IJK] \underline{v}_{PQW}$$

$$[PQW2IJK] = \begin{bmatrix} c_\Omega c_\Omega - s_\Omega s_\Omega c_i & -c_\Omega s_\Omega - s_\Omega c_\Omega c_i & s_\Omega s_i \\ s_\Omega c_\Omega + c_\Omega s_\Omega c_i & -s_\Omega s_\Omega + c_\Omega c_\Omega c_i & -c_\Omega s_i \\ s_\Omega s_i & c_\Omega s_i & c_i \end{bmatrix}$$

Where  $c_\Omega = \cos(\Omega)$ ,  $s_\Omega = \sin(\Omega)$ ,  $c_i = \cos(i)$  and  $s_i = \sin(i)$ .

## 2.2 Dynamic Equations

In order to study the motion of an asteroid or any other celestial body it is important to accurately define the dynamic equations that fully represent our system. In our case a Newtonian-Keplerian approach has been used to formulate the differential equations that fully describe the *six degrees of freedom (DOF)* in the two-body system, allowing us to calculate the state vector and the attitude of the asteroid, in the following way:

$$\dot{\underline{r}} = \underline{v} \quad (2.28)$$

$$\ddot{\underline{r}} = -\frac{\mu}{r^3}\underline{r} + \underline{a}_p \quad (2.29)$$

$$\underline{a}_p = \frac{\sum \underline{f}_p}{m} \quad (2.30)$$

$$\dot{\underline{q}} = H(\underline{q})\underline{\omega} \quad (2.31)$$

$$\mathbf{I} \cdot \dot{\underline{\omega}} + \underline{\omega} \times (\mathbf{I} \cdot \underline{\omega}) = \underline{\tau} \quad (2.32)$$

$$\underline{\tau} = \sum \underline{\tau}_p = \sum (\underline{c}_p \times \underline{f}_p) \quad (2.33)$$

Where  $\underline{r}$  and  $\underline{v}$  form the state vector, they are the position and velocity of respectively.  $\underline{q}$  and  $\underline{\omega}$  are the attitude quaternion and angular velocity correspondingly.  $\mathbf{I}$  is the moment of inertia tensor.  $\underline{\tau}$  is the total torque.  $\underline{f}_p$  and  $\underline{\tau}_p$  are the external perturbations, in the fashion of forces and torques respectively.  $\underline{a}_p$  is the acceleration vector due to the combined effect of all the external forces. And  $H(\underline{q})$  is defined by:

$$H(\underline{q}) = \frac{1}{2} \begin{bmatrix} \underline{q}_v^\times + q_3 I_{3 \times 3} \\ -\underline{q}_v^T \end{bmatrix}$$

Where  $I_{3 \times 3}$  is the  $3 \times 3$  identity matrix and  $\underline{q}_v^\times$  is the cross-product matrix given by:

$$\underline{q}_v^\times = \begin{bmatrix} 0 & -q_2 & q_1 \\ q_2 & 0 & -q_0 \\ -q_1 & q_0 & 0 \end{bmatrix}$$

The DSENDSEdu platform simplifies our problem, due to the fact that it has been intrinsically designed to solve these differential equations and obtain at any point the state vector and the attitude of the body. Our scope will be that of correctly defining the initial settings and external inputs of our system.

## 2.3 External Perturbations on Asteroids

The motion of the asteroid is subject to external forces and torques that determine the *forced response* of the system. They are classified into gravitational and non-gravitational perturbations, depending on its nature. The main forces and torques considered as perturbations are:

- Solar Radiation Pressure: non gravitational perturbation caused by the electromagnetic radiation of the Sun. The photon flux originating from the Sun produces an effective pressure[2] on the celestial bodies that intercept it. This pressure is further traduced into a force and torque perturbation. Its concept will be deepen in Chapter 3.
- Planetary Gravity: gravitational perturbation caused by a *third-body* gravitational potential. It has particular importance during close *flybys* of Planets or their natural satellites. Its theory will be expanded in Chapter 4.
- *Yarkovsky* and *YORP* effects: the Yarkovsky and YORP (Yarkovsky-O’Keefe-Radzievskii-Paddack) effects are thermal radiation forces and torques that cause small-bodies to undergo semi-major axis drift and spin vector modifications, respectively, as a function of their spin, orbit, and material properties[4].

The Yarkovsky effect is caused by the anisotropic emission of thermal photons. The side of the asteroid facing the Sun heats up then reradiates the photons, thus exchanging momentum. Since the small-body has thermal inertia, the temperature distribution is not symmetrical and therefore the resultant force has two components, one radially outward the Sun and the other in the direction of the orbit, causing *prograde* rotating asteroids to spiral outward[4].

The reflection and reemission of sunlight from an asteroid’s surface can also produce a net thermal torque on asteroids with irregular shapes, this effect is known as the YORP effect. Over time, these torques can affect the spin rate and obliquities of small bodies in the solar system[4].

- Solar Wind: the Sun is losing mass in form of the solar wind, which has affected its evolution from its birth and will continue to do so until its death. The surface of the Sun is called the photosphere, above which lies the Sun’s atmosphere, known as the corona. The solar wind forms in the corona and is caused by high pressure in the corona relative to the low pressure far from the Sun in the interstellar medium. Solar wind is an ionized gas made up primarily of protons and electrons with minor ions in amounts similar to those in the corona. The rotation of the sun results in the lines of magnetic flux in the solar wind being drawn into *Archimedian spirals*<sup>1</sup>. This is because the Sun revolves once every  $\sim 25.5$  days while it takes solar wind several days to reach 1 AU[24]. Therefore the Sun rotates through a significant angle during the time it takes the solar wind to reach an asteroid.

In Tables 2.3 and 2.4 an overview of the probabilistic error of all the important perturbations for a Near Earth environment is presented[12]. The survey is applied to the Galileo spacecraft, but for our analysis it provides trustworthy information of the contribution of the different perturbations in the specific environment of a NEA.

It is assumed that all of the error sources or the combined effect of the error sources have a normal (Gaussian) distribution[12]. The *mean* and *three standard deviations* ( $3\sigma$ ) values are displayed. As can be seen in Figure 2.6, 99.73% of values are within three standard deviations of the mean, therefore we have a good approximation of the actual value of the external perturbations.

Source	Near Earth ( $10R_E$ )	
	Mean	$3\sigma$
Solar Radiation Pressure	$9.0 \times 10^{-5}$	$2.6 \times 10^{-5}$
Planet Thermal Radiation	$7.8 \times 10^{-8}$	$5.2 \times 10^{-8}$
Solar Wind	$3.1 \times 10^{-8}$	$1.6 \times 10^{-8}$
Newtonian Drag	$7.9 \times 10^{-11}$	$2.4 \times 10^{-10}$

**Table 2.3:** Probabilistic error modelling of environmental forces on the Galileo spacecraft [N] [12]

Our attention will now be focused on the effects of SRP and Planetary Gravity (Gravity Gradient), as they are the main sources of external perturbation to the

---

<sup>1</sup>An Archimedean spiral is a plane curve generated by a point moving away from or toward a fixed point at a constant rate while the radius vector from the fixed point rotates at a constant rate.[15]

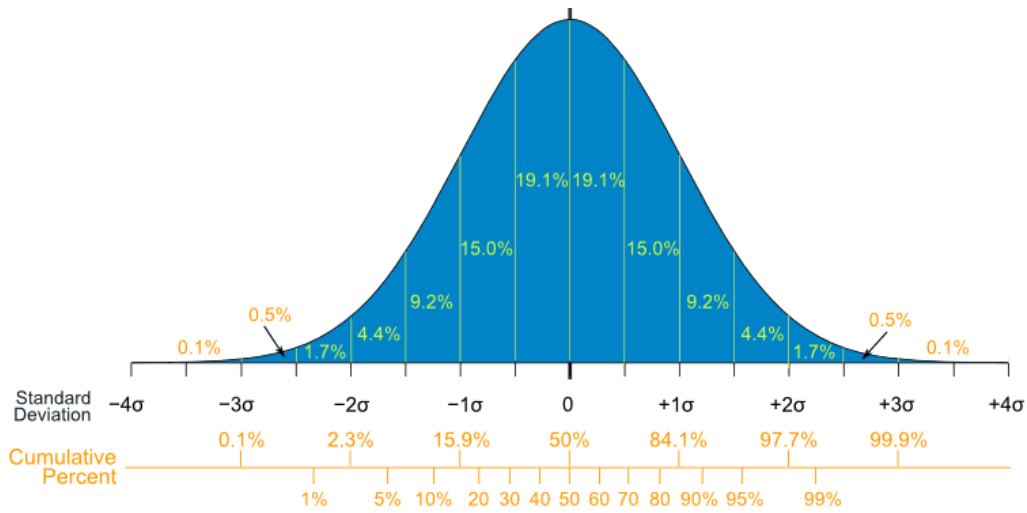


**Figure 2.6:** "Bell Curve" Standard Normal (Gaussian) Distribution [20]

Source	Near Earth ( $10R_E$ )	
	Mean	$3\sigma$
Solar Radiation Pressure	0	$3.2 \times 10^{-7}$
Planet Thermal Radiation	$3.5 \times 10^{-8}$	$2.5 \times 10^{-8}$
Solar Wind	0	$2.8 \times 10^{-10}$
Newtonian Drag	$3.4 \times 10^{-11}$	$1.1 \times 10^{-10}$
Gravity Gradient Torque	$3.2 \times 10^{-7}$	$3.9 \times 10^{-8}$

**Table 2.4:** Probabilistic error modelling of secular precessional torques on the Galileo spacecraft [Nm] [12]

dynamics of the asteroid. They are at least one order of magnitude larger than the rest of the perturbations (in the case of the Gravity Gradient and SRP induced torques in Table 2.4), and three orders of magnitude larger than the others (in the case of SRP force in Table 2.3) in the case of the Galileo spacecraft under the condition of interest.

# Chapter 3

## Solar Radiation Pressure

In this chapter the reader will be introduced to some models of Solar Radiation Pressure (SRP). These models represent a physical approach for calculating the SRP force and torque acting on an asteroid. The complexity of such models greatly depend on the magnitude of the uncertainty and therefore how similar to the reality is the model meant to be. The models here presented were implemented into appropriate Python functions that feed up the overall simulation of the asteroid's dynamics.

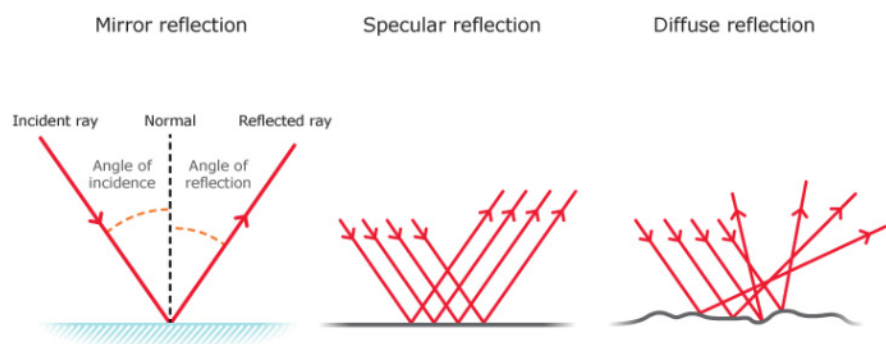


**Figure 3.1:** Components of Reflection [18]

SRP is the largest non conservative, non-gravitational perturbation for an asteroid. The radiation produced by the Sun exerts a pressure in every surface that intercepts it[25], and therefore it is important to measure its effect on the orbital dynamics of asteroids. This pressure is normally relatively "small", but it is the

cumulative effect over sufficiently long periods of time that make it significant[10], in particular for NEA that do not experience strong gravitational dynamics or other significant environmental forces. Sunlight has both energy and momentum, consequently when a photon is absorbed or reflected, momentum is exchanged[2]. Resultant force is a function of the exposed area and surface characteristics, which determine how the incoming photons are specularly reflected, diffusely reflected or absorbed.

### 3.1 Rigid Body Model

As a start the model of D.A. Vallado[25] of SRP for a rigid body is presented. This basic model, as will be seen additionally in the rest of the models, strongly depends on the area-to-mass ratio of the body. This give us a hint on what should be our scope when determining the relevance of the SRP effect on the orbital dynamics of a natural satellite. The structure of the equation is given as:

$$\underline{a}_{SR} = -\frac{p_{SR}C_R A_\odot}{m} \frac{\underline{r}_{ast\odot}}{|\underline{r}_{ast\odot}|} \quad (3.1)$$

Where  $C_R$  is the single reflectivity coefficient,  $p_{SR}$  is the SRP coefficient, and  $A_\odot$  is the exposed area to the sun. And the position vector defined in an inertial reference frame is written as:

$\underline{r}_{ast\odot}$ : position vector between asteroid and sun

$|\underline{r}_{ast\odot}|$ : magnitude of the position vector

$\hat{\underline{r}}_{ast\odot} = \frac{\underline{r}_{ast\odot}}{|\underline{r}_{ast\odot}|}$ : unit vector pointing to the Sun (incident vector line)

Now, as showed in Figure 3.1, we consider the case for different components of reflection and absorption. From this analysis we obtain the following equations:

$$\underline{f}_a = -p_{SR}C_{Ra}A_\odot \cos(\phi_{inc}) \hat{s} \quad (3.2)$$

$$\underline{f}_{rs} = -2p_{SR}C_{Rs}A_\odot \cos^2(\phi_{inc}) \hat{n} \quad (3.3)$$

$$\underline{f}_{rd} = -p_{SR}C_{Rd}A_\odot \cos(\phi_{inc}) \left( \frac{2}{3} \hat{n} + \hat{s} \right) \quad (3.4)$$

Where  $\phi_{inc}$  is the solar-incidence angle,  $\hat{s}$  is the unit vector pointing in the opposite direction of the incident beam, and  $\hat{n}$  is the unit vector normal to the cross-sectional area.  $C_{Ra}$ ,  $C_{Rs}$  and  $C_{Rd}$  are the coefficients of absorption, specular

and diffuse reflectivities respectively. The summation of these coefficients must be equal to one ( $C_{Ra} + C_{Rs} + C_{Rd} = 1$ ).

Adding the previous terms of force in Equations 3.2, 3.3 and 3.4, and assuming a Lambertian diffusion (ideal diffusely reflecting surface) we find compact equations for the SRP Force and Torque, defined by:

$$\underline{f}_{SRP} = -p_{SR}A_{\odot}\cos(\phi_{inc}) \left( 2 \left( \frac{C_{Rd}}{3} + C_{Rs}\cos(\phi_{inc}) \right) \hat{n} + (1 - C_{Rs})\hat{s} \right) \quad (3.5)$$

$$\underline{\tau}_{SRP} = (\underline{r}_{CoP} - \underline{r}_{ast\odot}) \times \underline{f}_{SRP} \quad (3.6)$$

Where  $\underline{r}_{CoP}$  is the position of Center of Pressure (CoP) of the body, and  $\underline{r}_{ast\odot}$  corresponds to the position of the CoM of the asteroid.

## 3.2 Finite Elements of Area Model

In this section the SRP is modelled in a more in depth way, instead of having an estimated cross-sectional area illuminated by the Sun rays, the total area exposed to the Sun is defined as the addition of a number of finite areas. Following up the P.C. Hughes[10] model for SRP Force and Torque are presented:

$$\underline{f} = p[(\sigma_a + \sigma_{rd})A_p\hat{s} + \frac{2}{3}\sigma_{rd}\underline{A}_p + 2\sigma_{rs}\underline{A}_{pp}] \quad (3.7)$$

$$\underline{g} = p[(\sigma_a + \sigma_{rd})\underline{c}_p^x\hat{s} + \frac{2}{3}\sigma_{rd}\underline{G}_p + 2\sigma_{rs}\underline{G}_{pp}] \quad (3.8)$$

Where  $A_p$ ,  $\underline{c}_p$ ,  $\underline{A}_p$ ,  $\underline{A}_{pp}$ ,  $\underline{G}_p$  and  $\underline{G}_{pp}$  are given as:

$$A_p = \iint H(\cos(\theta))\cos(\theta)dA \quad (3.9)$$

$$A_p\underline{r}_{CoP} = \iint H(\cos(\theta))\cos(\theta)\underline{r}dA \quad (3.10)$$

$$\underline{A}_p = \iint H(\cos(\theta))\cos(\theta)d\underline{A} \quad (3.11)$$

$$\underline{A}_{pp} = \iint H(\cos(\theta))\cos^2(\theta)d\underline{A} \quad (3.12)$$

$$\underline{G}_p = \iint H(\cos(\theta))\cos(\theta)\underline{r}^x d\underline{A} \quad (3.13)$$

$$G_{pp} = \oint H(\cos(\theta)) \cos^2(\theta) \underline{r}^x d\underline{A} \quad (3.14)$$

Where  $\theta$  is the incident angle.  $H(\cos(\theta))$  is the Heaviside function ( $H(\cos(\theta)) = 1$  when  $\cos(\theta) > 0$ ), it limits the calculation of the SRP to the areas that are exposed to the sun, specifically when the incident angle is  $-\frac{\pi}{2} \leq \theta \leq \frac{\pi}{2}$ .

And the relative position  $\underline{r} = \underline{r}_{CoP} - \underline{r}_{CoM}$ , where  $\underline{r}_{CoP}$  is the location of the CoP,  $\underline{r}_{CoM}$  is the location of the CoM of the asteroid.

The difference between the total CoP and the CoM is what creates the applied torque to the body. If both of them would be located in the same position with respect to the body the applied torque would be zero.

The differential element of area  $d\underline{A} = \hat{n}dA$  can be decomposed in magnitude and direction.

The parameters  $\sigma_a$ ,  $\sigma_{rd}$  and  $\sigma_{rs}$  are respectively the coefficients for absorption, diffuse reflection and specular reflection.

### 3.3 Solar Sail Model

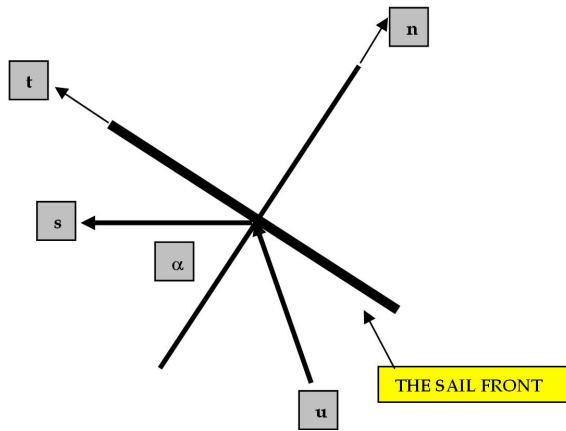


**Figure 3.2:** Diagram of vectors for the non-ideal solar sail[21]

In this section the model of SRP for a *solar sail* developed by C.R. McInnes[14] is considered. The momentum carried by individual photons is vanishingly small and therefore in order to intercept a large number of photons the area of the sail must be substantial. Moreover, in order to create the highest possible acceleration the solar sail must have low mass. There is a similarity between the modelling the dynamics of a solar sail and the dynamics of a small-body (particularly for the calculation of

the SRP), both of them possess high area-to-mass ratio and furthermore they must be almost perfect reflectors for the SRP to be appreciable.

Unfortunately, as considered in the previous model, the SRP force is not generated by a surface with a perfect reflectivity. Therefore as can be seen in Figure 3.2 the force exerted by a non-ideal solar sail is obtained by considering reflection, absorption and re-radiation by the sail.

The equations of the SRP exerted by the sail are determined by:

$$\underline{f_n} = pA((1 + \tilde{r}s)\cos^2\theta + B_f(1 - s)\tilde{r}\cos\theta + (1 - \tilde{r})\frac{\varepsilon_f B_f - \varepsilon_b B_b}{\varepsilon_f + \varepsilon_b}\cos\theta)\hat{n} \quad (3.15)$$

$$\underline{f_t} = pA(1 - \tilde{r}s)\cos\theta\sin\theta\hat{t} \quad (3.16)$$

For this model  $\tilde{r}$  is the reflection coefficient,  $s$  is the fraction of specularly reflected force,  $\hat{n}$  is the unit vector normal to the sail surface,  $\hat{t}$  is the transverse unit vector to that surface,  $B_f$  and  $B_b$  are the coefficient that account for a non-Lambertian surface in the front and back of the sail.  $\varepsilon_f$  and  $\varepsilon_b$  are the front and back emissivities.

Limiting our model to only front sail surfaces, the equation in the normal direction changes as follow:

$$\underline{f_n} = pA((1 + \tilde{r}s)\cos^2\theta + B_f(1 - s)\tilde{r}\cos\theta + (1 - \tilde{r})B_f\cos\theta)\hat{n} \quad (3.17)$$

Which for a coefficient  $B_f = \frac{2}{3}$  (Lambertian diffusion) turns out to be a similar equation as the previous models.

The only notable difference between models is the notation used to describe the coefficients. For this reason and for a future test validation a coefficient relation between models is presented:

$$\tilde{r} = \sigma_{rd} + \sigma_{rs} = 1 - \sigma_a \quad (3.18)$$

$$s = 1 - \sigma \quad (3.19)$$

$$\sigma_{rd} = \sigma(1 - \sigma_a) \quad (3.20)$$

$$\sigma_{rs} = (1 - \sigma)(1 - \sigma_a) \quad (3.21)$$

Where  $\sigma_a$  is the fraction absorbed and  $\sigma$  is the fraction that is diffusely reflected, whereas  $(1 - \sigma)$  represents the fraction specularly reflected.

### 3.4 Implemented Solar Radiation Pressure Model

In this section simplified equations to calculate the total SRP force and torque are derived from the P.C. Hughes[10].

Replacing 3.9, 3.10, 3.11, 3.12, 3.13 and 3.14 in 3.7 we obtain:

$$\begin{aligned} \underline{f} &= p[(\sigma_a + \sigma_{rd}) \iint H(\cos\theta) \cos\theta dA \hat{s} + \frac{2}{3} \sigma_{rd} \iint H(\cos\theta) \cos\theta dA \hat{A} + 2\sigma_{rs} \iint H(\cos\theta) \cos^2\theta dA] \\ \underline{f} &= \iint p[(\sigma_a + \sigma_{rd}) H(\cos\theta) \cos\theta \hat{s} + \frac{2}{3} \sigma_{rd} H(\cos\theta) \cos\theta \hat{n} + 2\sigma_{rs} H(\cos\theta) \cos^2\theta \hat{n}] dA \\ \underline{f} &= \iint pH(\cos\theta) \cos\theta [(\sigma_a + \sigma_{rd}) \hat{s} + (\frac{2}{3} \sigma_{rd} + 2\sigma_{rs} \cos\theta) \hat{n}] dA \end{aligned} \quad (3.22)$$

Equation 3.22 is in fact the total SRP Force. Using this equation and the relative distance between the CoP and the CoM, we derive an expression for the the total SRP Torque perturbing the asteroid, as follows:

$$\underline{f}_{SRP} = \iint pH(\cos(\theta)) \cos(\theta) [(\sigma_a + \sigma_{rd}) \hat{s} + (\frac{2}{3} \sigma_{rd} + 2\sigma_{rs} \cos(\theta)) \hat{n}] dA \quad (3.23)$$

$$\underline{\tau}_{SRP} = \underline{r} \times \underline{f}_{SRP} \quad (3.24)$$

$$\underline{r} = \underline{r}_{CoP} - \underline{r}_{CoM}$$

# Chapter 4

## Planetary Gravity

In the unperturbed Keplerian motion of an asteroid about the Sun, it is assumed that the dynamics of the small-body are only defined by the acceleration due to the gravity of the Sun (this concept was established in Section 2.1 as the free response of the system). In reality other planets also introduce a perturbing acceleration on the body, defined as third-body gravitational perturbations. They are usually small comparing to that of the Sun and therefore its effect is neglected. However such is not the case of our problem.

In this chapter the reader will be introduced to the gravitational acceleration exerted by other Planets or their natural satellites on asteroids. Particularly, since the subject of our study are NEA, its close flyby to the Earth and Moon makes their effect considerable compared to that of the rest of the Planets. Therefore the importance of describing the aforementioned effects in a more accurate way.

### 4.1 Gravitational Potential

When calculating the gravitational potential of a planet it is often assumed that the total mass of the planet (i.e. Earth), is concentrated in the center of the coordinate system, and the gravitational law [16] is written by:

$$\ddot{\underline{r}} = -\frac{GM}{r^3}\underline{r} \quad (4.1)$$

Where  $M$  is the mass of the Planet, and the mass of the asteroid is negligible compared to the former (analogue to Equation 2.18).  $\underline{r}$  is the position of the CoM of the asteroid. Equation 4.1 could be used to compute the gravitational acceleration felt by the small-body at a position  $\underline{r}$ . However such is not the case, since the shape of Planets is aspherical, thus the need to model it in a different way, taking into account its oblateness and all of the other variations from a spherical model. For

for this purpose a more realistic model is presented. This model involves the gradient of the gravitational potential ( $V$ ) of the body[16] in the following way:

$$\ddot{\underline{r}} = \nabla V \quad (4.2)$$

with

$$V = G \int \frac{dm}{|\underline{r} - \underline{s}|} \quad (4.3)$$

Equation 4.3 applies for an arbitrary mass distribution and  $dm = \rho(\underline{s})d^3\underline{s}$  is the mass element. Where  $\underline{s}$  is the position of the individual mass element with respect to the CoM, and  $\rho(\underline{s})$  is the density of the body.

#### 4.1.1 Spherical Harmonics

The fraction within the integral in Equation 4.3 is expanded in a series of Legendre Polynomials[16], as follows:

$$\frac{1}{|\underline{r} - \underline{s}|} = \frac{1}{r} \sum_{n=0}^{\infty} \left(\frac{s}{r}\right)^n P_n(\cos(\gamma))$$

Where  $\gamma = \frac{\underline{r} \cdot \underline{s}}{rs}$  is the angle between  $\underline{r}$  and  $\underline{s}$ , and the Legendre polynomial of degree  $n$  ( $P_n$ ) is written as:

$$P_n(\theta) = \frac{1}{2^n n!} \frac{d^n}{d\theta^n} (\theta^2 - 1)^n$$

And the associated Legendre polynomials of degree  $n$  and order  $m$  are defined as:

$$P_{nm}(\theta) = (1 - \theta^2)^{m/2} \frac{d^m}{d\theta^m} P_n(\theta)$$

Introducing the spherical coordinates  $(r, \theta, \lambda)$ , with radius  $r$ , longitude  $\lambda$ , and latitude  $\theta$ , it is possible to write the planetary gravitational potential in the following form[9]:

$$V(r, \theta, \lambda) = \frac{GM}{r} + \frac{GM}{r} \sum_{n=2}^{n_{max}} \left(\frac{a}{r}\right)^n \sum_{m=0}^n \left(\bar{C}_{nm} \cos(m\lambda) + \bar{S}_{nm} \sin(m\lambda)\right) \bar{P}_{nm}(\theta) \quad (4.4)$$

Where  $\bar{C}_{nm}$  and  $\bar{S}_{nm}$  are the fully-normalised, unit-less, spherical harmonic coefficients of the Planet's gravitational potential, and  $\bar{P}_{nm}(\theta)$  are the normalised associated Legendre polynomials.

### 4.1.2 Normalised Associated Legendre Functions

In this section a method[9] of forward recursions for the calculation of the normalised associated Legendre functions (polynomials)  $\bar{P}_{nm}(\theta)$  is presented. The full normalisation is given by:

$$\bar{P}_{nm}(\theta) = \sqrt{\frac{k(2n+1)(n-m)!}{(n+m)!}} P_{nm}(\theta) \quad (4.5)$$

where  $k = 1$  for  $m = 0$  and  $k = 2$  for  $m > 0$ .

The full normalisation requires a recursion that computes non-sectoral ( $n > m$ ) from previously computed functions. The non-sectoral terms of  $\bar{P}_{nm}(\theta)$  are given as:

$$\bar{P}_{nm}(\theta) = a_{nm} t \bar{P}_{n-1,m}(\theta) - b_{nm} \bar{P}_{n-2,m}(\theta), \quad \forall n > m \quad (4.6)$$

where  $t = \cos(\theta)$

$$a_{nm} = \sqrt{\frac{(2n+1)(2n+1)}{(n-m)(n+m)}}$$

and

$$b_{nm} = \sqrt{\frac{(2n+1)(n+m-1)(n-m-1)}{(n-m)(n+m)(2n-3)}}$$

The sectoral ( $n = m$ ) terms  $\bar{P}_{0,0}(\theta) = 1$  and  $\bar{P}_{1,1}(\theta) = \sqrt{3}u$  serve as seed values for the recursion, where  $u = \sin(\theta)$ .

The higher degree and order terms of  $\bar{P}_{mm}(\theta)$  are computed as follow:

$$\bar{P}_{mm}(\theta) = u \sqrt{\frac{2m+1}{2m}} \bar{P}_{m-1,m-1}(\theta), \quad \forall m > 1 \quad (4.7)$$

## 4.2 Gravitational Acceleration Vector

The gravitational acceleration vector,  $\underline{g}$ , is calculated as the first partial derivative of the Gravitational Potential,  $V$ , with respect to the planet-fixed position vector,  $\underline{r}$ . A method found in [7] for calculating  $\underline{g}$  is presented:

$$\underline{g} \equiv \frac{\partial V}{\partial \underline{r}} \quad (4.8)$$

Where:

$$\underline{r} = \begin{bmatrix} x_1 \\ x_2 \\ x_3 \end{bmatrix}$$

$$\hat{r} = \frac{\underline{r}}{r}$$

$$\Lambda \equiv \Gamma + \frac{x_3 H}{r}$$

$$J \equiv \sum_{n=2}^{n_{max}} \left( \frac{a}{r} \right)^n J_n$$

$$K \equiv \sum_{n=2}^{n_{max}} \left( \frac{a}{r} \right)^n K_n$$

$$H \equiv \sum_{n=2}^{n_{max}} \left( \frac{a}{r} \right)^n H_n$$

$$\Gamma \equiv 1 + \sum_{n=2}^{n_{max}} \left( \frac{a}{r} \right)^n \Gamma_n$$

Defining the  $n$  variables as:

$$J_n \equiv \sum_{m=1}^n m \frac{\bar{P}_{n,m}}{r^{m-1}} (\bar{C}_{n,m} C_{m-1} + \bar{S}_{n,m} S_{m-1})$$

$$K_n \equiv - \sum_{m=1}^n m \frac{\bar{P}_{n,m}}{r^{m-1}} (\bar{C}_{n,m} S_{m-1} - \bar{S}_{n,m} C_{m-1})$$

$$H_n \equiv \bar{C}_{n,0} \bar{P}_{n,1} + \sum_{m=1}^n \frac{\bar{P}_{n,m+1}}{r^m} (\bar{C}_{n,m} C_m + \bar{S}_{n,m} S_m)$$

$$\Gamma_n \equiv \bar{C}_{n,0} (n+1) \bar{P}_{n,0} + \sum_{m=1}^n (1+n+m) \frac{\bar{P}_{n,m}}{r^m} (\bar{C}_{n,m} C_m + \bar{S}_{n,m} S_m)$$

and

$$C_m \equiv \rho^m \cos(m\lambda)$$

$$S_m \equiv \rho^m \sin(m\lambda)$$

$$\rho^2 \equiv {x_1}^2 + {x_2}^2$$

We can write a simple and compact vector equation for the gravitational acceleration:

$$\mathbf{g} = -\frac{\mu}{r^2} \left( \Lambda \hat{r} - \begin{bmatrix} J \\ K \\ H \end{bmatrix} \right) \quad (4.9)$$

### 4.3 Earth Gravitational Model

As previously discussed in the case of the study of the orbital dynamics of NEA, it is fundamental to measure the perturbing effect caused by the gravitational potential of Earth. For this reason the Earth Gravitational Model EGM2008[19] is adopted. The EGM2008[19] model is complete to degree and order 2159. This model represents the most complete description of the Earth's gravitational model in spherical harmonics. The ASCII file contains 2401333 formatted records with the following coefficients:

$$\{n, m, \bar{C}_{nm}, \bar{S}_{nm}, \text{sigma}\bar{C}_{nm}, \text{sigma}\bar{S}_{nm}\}$$

Where  $n$ , is the degree,  $m$ , the order,  $\bar{C}_{nm}$  and  $\bar{S}_{nm}$  are the normalised spherical harmonic coefficients of the gravitational potential, and  $\text{sigma}\bar{C}_{nm}$  and  $\text{sigma}\bar{S}_{nm}$ , their associated error standard deviations.

The scaling parameters (standard gravitational parameter,  $GM$ , and the equatorial radius,  $a$ ) associated with this model have numerical values:

$$GM = 3986004.415 \times 10^8 \left[ \frac{m^3}{s^2} \right]$$

$$a = 6378136.3 [m]$$

For simplicity I created a truncated file (`EGM2008_120`) that contains the normalised spherical harmonic coefficients up to the 120th degree and order. This file serves as the input of our model due to the fact that with higher degree and order increases the computational effort. The results from a test of the model up to the 20th degree and order, with position vector  $\underline{r} = [0, 0, -6381.751E3]$ , are presented:

<b>n</b>	<b>V</b> [ $\frac{\text{Nm}}{\text{kg}}$ ]	<b>g</b> [ $\frac{\text{m}}{\text{s}^2}$ ]
3	62459416.154	(2.245017e-18, -0.0, 9.755439150056413)
4	62459416.154	(2.245015e-18, 1.073547e-23, 9.755439171420868)
5	62459416.154	(2.234156e-18, 1.073547e-23, 9.755579372118891)
6	62459416.154	(2.245231e-18, 2.172461e-20, 9.755439283003227)
7	62459416.154	(2.225674e-18, 2.569082e-20, 9.755683211368497)
8	62459416.154	(2.214619e-18, 2.043162e-20, 9.755819689420921)
9	62459416.154	(2.212929e-18, 2.016738e-20, 9.755840385846357)
10	62459416.154	(2.221663e-18, 1.259672e-20, 9.75573408029359)
11	62459416.154	(2.222447e-18, 1.607862e-20, 9.75572457575225)
12	62459416.154	(2.214993e-18, 1.263204e-20, 9.75581447903136)
13	62459416.154	(2.215362e-18, 2.073509e-20, 9.755810051547115)
14	62459416.154	(2.213559e-18, 1.195743e-20, 9.75583166226041)
15	62459416.154	(2.210959e-18, 1.031292e-20, 9.755862738632983)
16	62459416.154	(2.209396e-18, 1.739376e-20, 9.755881374822108)
17	62459416.154	(2.206491e-18, 1.582666e-20, 9.755915959760905)
18	62459416.154	(2.211131e-18, 1.736107e-20, 9.755860821214721)
19	62459416.154	(2.214331e-18, 1.937496e-20, 9.755822848474203)
20	62459416.154	(2.214976e-18, 1.989379e-20, 9.755815219534897)

**Table 4.1:** Variation of gravitational potential and gravitational acceleration of the Earth with the degree

## 4.4 Moon Gravitational Model

The other considerable external gravitational perturbation for NEA is the gravitational acceleration generated by the Moon. In a similar way to the previous section, we use the Lunar Prospector mission data LP150[13]. The LP150[13] model is complete to the 150th degree and order. The ASCII file contains 11473 formatted records with the following coefficients:

$$\{n, m, \bar{C}_{nm}, \bar{S}_{nm}, \text{sigma}\bar{C}_{nm}, \text{sigma}\bar{S}_{nm}\}$$

Where  $n$ , is the degree,  $m$ , the order,  $\bar{C}_{nm}$  and  $\bar{S}_{nm}$  are the normalised spherical harmonic coefficients of the gravitational potential, and  $\text{sigma}\bar{C}_{nm}$  and  $\text{sigma}\bar{S}_{nm}$ , their associated error standard deviations.

The scaling parameters (standard gravitational parameter,  $GM$ , and the equatorial radius,  $a$ ) associated with this model have numerical values:

$$GM = 0.49028002380000 \times 10^{13} \left[ \frac{m^3}{s^2} \right]$$

$$a = 1738000.0 [m]$$

The results of a test of the model up to the 20th degree and order, with position vector  $\underline{r} = [0, 0, 1738000.0]$ , are presented:

<b>n</b>	<b>V</b> [ $\frac{\text{Nm}}{\text{kg}}$ ]	<b>g</b> [ $\frac{\text{m}}{\text{s}^2}$ ]
3	2820943.75029	(-0.0, -0.0, -1.6221080516181843)
4	2820943.75029	(-0.0, -0.0, -1.6221075428218674)
5	2820943.75029	(-0.0, -0.0, -1.6220285395287453)
6	2820943.75029	(-0.0, -0.0, -1.6224252246161879)
7	2820943.75029	(-0.0, -0.0, -1.6223695327499759)
8	2820943.75029	(-0.0, -0.0, -1.6223970597650141)
9	2820943.75029	(-0.0, -0.0, -1.6221939155996075)
10	2820943.75029	(-0.0, -0.0, -1.6222233553284742)
11	2820943.75029	(-0.0, -0.0, -1.6220696886369494)
12	2820943.75029	(-0.0, -0.0, -1.6218769635476218)
13	2820943.75029	(-0.0, -0.0, -1.621945771201444)
14	2820943.75029	(-0.0, -0.0, -1.622025384358224)
15	2820943.75029	(-0.0, -0.0, -1.622145487058275)
16	2820943.75029	(-0.0, -0.0, -1.6221011972293156)
17	2820943.75029	(-0.0, -0.0, -1.6221490768703688)
18	2820943.75029	(-0.0, -0.0, -1.621871011647331)
19	2820943.75029	(-0.0, -0.0, -1.621811282914)
20	2820943.75029	(-0.0, -0.0, -1.6217564652529954)

**Table 4.2:** Variation of Moon’s gravitational potential and gravitational acceleration with the degree



# Chapter 5

## Shape Model of Asteroids

In this chapter the reader will be introduced to the shape model of asteroids and its structure. The mentioned shape must be adequate with the models of the main external perturbations previously discussed, and will be subsequently used with major importance in the simulation of the dynamics of asteroids. For this purpose the entire surface of the small-body is divided into finite elements of area, fitting the model of SRP presented in Section 3.2. In order to accomplish this, the asteroid is modelled as a polyhedron-shaped body, a mesh containing flat facets and straight vertices. Each facet represents a finite area within the polyhedron and the vertices define the total area within each facet.

### 5.1 NASA Shape Models

In Figure 5.1 a model of asteroid (1620) Geographos is presented. This and several other shape models can be found in NASA's Planetary Data System (<http://sbn.psi.edu/pds/archive/shape.html>). These shape models were derived using experimental data from radar or optical observations. Shape models typically have several thousands of surface triangular facets[5], increasing the number of facets increases the precision of the model but also increases the computational effort. For each asteroid there is a .obj (.tab) file with the following format:

```
v x1 y1 z1  
v x2 y2 z2  
v x3 y3 z3  
...  
f i1 j1 k1  
f i2 j2 k2  
f i3 j3 k3  
...
```

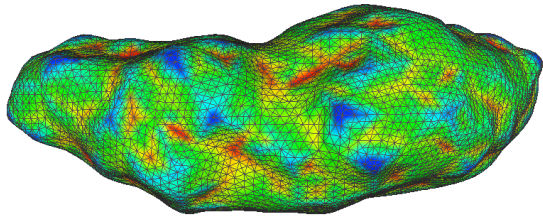


**Figure 5.1:** (1620) Geographos Radar-based Polyhedron Shape Model

Rows starting with letter  $v$  represent the  $x$ ,  $y$ , and  $z$ -axis coordinates of each vertex, whereas rows starting with letter  $f$  represent each triangular facet and  $i$ ,  $j$ , and  $k$  are the number of vertices that form the facet. The number of facets  $n_f$  and the number of vertices  $n_v$  are related by  $n_f = 2n_v - 4$ . The radar shape model of the asteroid (1620) Geographos shown in Figure 5.1 contains 8192 Vertices and 16380 Facets, which imply a great computational constraint. In fact when this model is used to measure the effects of SRP in the orbital and attitude dynamics of the small-body, the simulation runs slow. For this reason another approach has been used to model the asteroid's shape.

## 5.2 Gaussian Random Spheres

In this section the irregular shape of asteroids is modelled using Gaussian Random Spheres (GRS), in which a sphere is deformed using some key parameters in order to get the approximate shape of a real asteroid. A GRS is fully described by the mean radius and the covariance function of the logarithmic radius[17]. In the following, the

statistical-stochastic GRS model found in [17] is presented. The three-dimensional GRS is described by:

$$r(\vartheta, \phi) = a \exp \left[ s(\vartheta, \phi) - \frac{1}{2} \beta^2 \right] \quad (5.1)$$

$$s(\vartheta, \phi) = \sum_{l=0}^{\infty} \sum_{m=-l}^l s_{lm} Y_{lm}(\vartheta, \phi) \quad (5.2)$$

Where  $a$  and  $\beta$  are the mean radius and the standard deviation of the logradius, and  $Y_{lm}$ 's are the orthonormal spherical harmonics. The relative standard deviation of radius is  $\sigma = \sqrt{\exp(\beta)^2 - 1}$ .

The real and imaginary parts of the spherical harmonics coefficients  $s_{lm}$ ,  $m \geq 0$ , are independent Gaussian random variables with zero means and variances

$$\text{Var}(Re(s_{lm})) = (1 + \delta_{m0}) \frac{2\pi}{2l + 1} C_l$$

$$\text{Var}(Im(s_{lm})) = (1 - \delta_{m0}) \frac{2\pi}{2l + 1} C_l$$

The coefficients  $C_l \geq 0$  are the Legendre coefficients of the log radius covariance function  $\Sigma_s$ , and we may write the following equation:

$$\Sigma_s(\gamma) = \beta^2 C_s(\gamma) = \sum_{l=0}^{\infty} C_l P_l(\cos \gamma)$$

$$\sum_{l=0}^{\infty} C_l = \beta^2$$

In which  $C_s$  is the logradius correlation function, represented as:

$$C_s(\gamma) = \sum_{l=0}^{\infty} c_l P_l(\cos \gamma),$$

$$\sum_{l=0}^{\infty} c_l = 1$$

In order to implement the model, the series need to be truncated at a certain degree  $L$  high enough to maintain good precision. The two perpendicular slopes,  $s(\vartheta) = \frac{r_\vartheta}{r}$  and  $s(\phi) = \frac{r_\phi}{r}$ , are independent Gaussian random variables with zero mean, and standard deviation given by:

$$\rho = \sqrt{-\Sigma_s^{(2)}(0)}$$

Where  $\Sigma_s^{(2)}(0)$  is the second derivative of the covariance function with respect to  $\gamma$ . The correlation length  $\ell$  and correlation angle  $\Gamma$  are defined by:

$$\ell = \frac{1}{\sqrt{-C_s^{(2)}(0)}}$$

$$\Gamma = 2 \arcsin\left(\frac{1}{2}\ell\right)$$

Since the focus of the algorithm will be that of creating individual shapes, it is needed to define some intrinsic parameters of the relative shape. Defining the intrinsic expectation of a function  $f = f(\vartheta, \phi)$  as:

$$E(f) = \frac{1}{4\pi} \int_0^\pi \int_0^{2\pi} d\vartheta d\phi \sin(\vartheta) f(\vartheta, \phi) \quad (5.3)$$

Using Equation 5.3 it is possible to write an expression for the mean radius  $\tilde{a}$ , standard deviation of the radius  $\tilde{\sigma}$ , standard deviation of the logarithmic radius  $\tilde{\beta}$ , standard deviation of slopes  $\tilde{\rho}$  and correlation angle  $\tilde{\Gamma}$  as follows:

$$\tilde{a} = E(r) \quad (5.4)$$

$$\tilde{\rho}^2 = \frac{1}{\tilde{a}^2} [E(r^2) - E(r)^2] \quad (5.5)$$

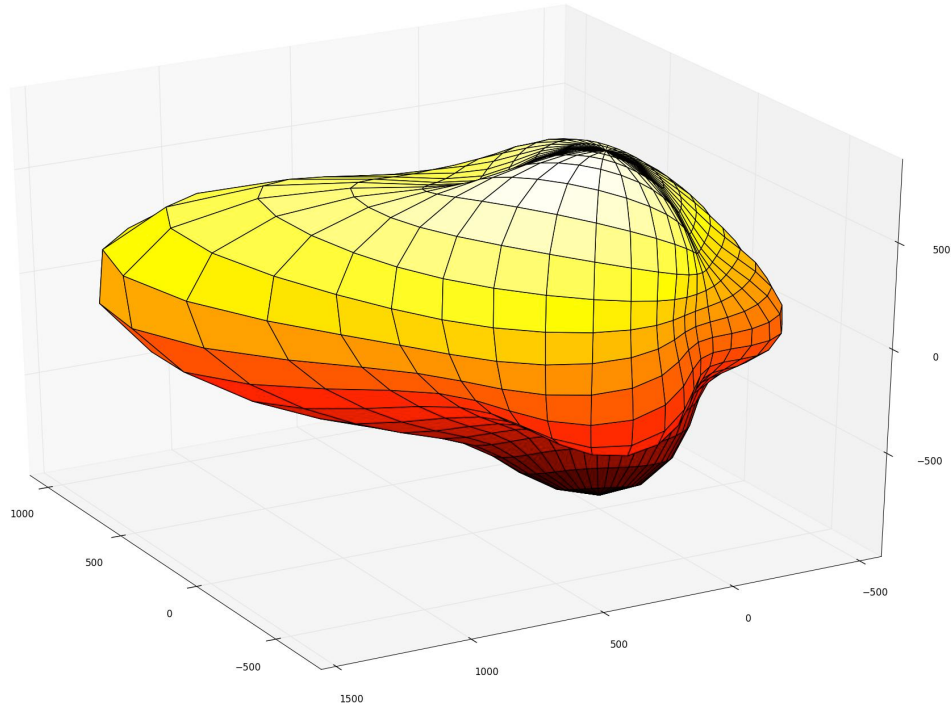
$$\tilde{\beta}^2 = E[(\log_e r)^2] - [E(\log_e r)]^2 \quad (5.6)$$

$$\tilde{\Gamma} = \frac{1}{2} E \left( \frac{r_\vartheta^2}{r^2} + \frac{r_\phi^2}{r^2 \sin^2 \vartheta} \right) \quad (5.7)$$

A Python routine has been implemented in order to generate GRS that recreate the individual shape of specific asteroids using the previous equations. The shape is stored into a .obj (.tab) file with the same format (facets-vertices) as the one defined in Section 5.1. Next it will be loaded into the main routine that computes the dynamics of the asteroid, and calculates the external forces and torques. At this point it will be particularly important to measure the total SRP acting on the body, since each facet provides a unique contribute to the total perturbation.

The GRS shape model of asteroid (1620) Geographos in Figure 5.2 has 861 vertices and 1568 facets, which is not as detailed when compared to the model displayed in Figure 5.1. Nevertheless it is still a good approximation of the real shape of the asteroid, and is more suitable for the testing of our SRP module. This model was accomplished in the routine selecting the origin as the CoM, constant density and statistical parameters found in [17], reported in Table 5.1.

Parameter	Value
Mean radius	$\tilde{a} = 1.08[\text{km}]$
Standard deviation of the radius	$\tilde{\sigma} = 0.319$
Standard deviation of slopes	$\tilde{\rho} = 0.546$
Correlation angle	$\tilde{\Gamma} = 33.1[\circ]$
Mean density	$\tilde{\rho} = 2.5[\frac{\text{g}}{\text{cm}^3}]$

**Table 5.1:** Gaussian random sphere (1620) Geographos parameters**Figure 5.2:** Polyhedron-based model of asteroid (1620) Geographos



# Chapter 6

## Tests and Results

In this chapter validating tests of the implemented Python[26] functions and their respective results will be reported. This chapter includes three main sections. The first one is dedicated to the test of the asteroid's dynamics and its behaviour over time, performing an assessment of the importance of the main external perturbations. The second one aims to validate the SRP model for a solar sail, contrasting the results with trusted bibliography. And the third one explores the concept of shadowing effects, and its relative importance when calculating the total SRP acting on an asteroid.

### 6.1 Asteroid Dynamics

In this section the results from the simulation of the orbital dynamics of asteroid (1620) Geographos will be presented. The following initial orbital parameters found in [5] are assumed:

Parameter	Value
Semi-major axis	$a = 1.24547 \text{ AU}$
Eccentricity	$e = 0.3354$
Inclination	$i = 13.34^\circ$
Argument of the perihelion	$\omega = 277.8^\circ$
Longitude of ascending node	$\Omega = 337.3^\circ$
True anomaly	$\nu = 10^\circ$

**Table 6.1:** Initial orbital elements of asteroid (1620) Geographos

The COE2rv Python[26] routine is used to transform from classical orbital elements to state vector, and the following initial state vector referred to the inertial

frame is found:

State vector	Value
Position	$r_0 = [-9385183996.563, -120902054235.237, -27307229916.384] m$
Velocity	$v_0 = [37304.738, -5110.708, 2295.700] \frac{m}{s}$

**Table 6.2:** Initial state vector of the CoM of asteroid (1620) Geographos

The following initial attitude have been chosen:

Attitude vector	Value
Quaternion	$q_0 = [0, 0, 0, 1]$
Initial angular velocity	$\omega_0 = [0.0, 0.0, 0.0] \frac{rad}{s}$

**Table 6.3:** Initial attitude of asteroid (1620) Geographos referred to the body frame

The previous parameters in Tables 6.1 and 6.3 plus the body properties in Table 6.4 form the initial setting needed to simulate the asteroid's gravitational orbit using the DSENDSEdu platform. The body properties of the asteroid are derived from the GRS model of asteroid (1620) Geographos presented in Figure 5.2, created with the parameters in Table 5.1 .

Property	Value
Mass	$6.2081 \times 10^{12} kg$
Volume	$2.4832 km^3$
Moment of Inertia	$\begin{bmatrix} 2.08434 \times 10^{18} & -1.67338 \times 10^{17} & 1.93765 \times 10^{17} \\ -1.67338 \times 10^{17} & 1.77484 \times 10^{18} & -3.09413 \times 10^{17} \\ 1.93765 \times 10^{17} & -3.09413 \times 10^{17} & 2.24548 \times 10^{18} \end{bmatrix} kg \cdot m^2$

**Table 6.4:** Body properties of asteroid (1620) Geographos

From now on the blue curves display the results of the DSENDSEdu simulation of the gravitational dynamics of the asteroid while the red curves include the effect of SRP force and torque acting on the small-body. In Figure 6.1 the position of the CoM ( $r$ ) of asteroid (1620) Geographos is displayed. The simulation time has been selected as  $5 \times 10^8 s \approx 1.5844 yr$ , allowing us to visualise the motion of the asteroid over a complete orbit, since the orbital period of (1620) Geographos is about 1.39yr. Figure 6.1 shows the orbital motion of the CoM of the asteroid, one curve displays the free-response of the system (dynamics of the asteroid defined only by the Sun's gravitational force) while the other includes the perturbation effect of the SRP. The

reason for their overlapping is that the variation of the orbital parameters is small over one orbit and therefore the impact of SRP is not visible. A more specific look at the state and attitude vectors, orbital elements and perturbation in orbital elements will provide us the expected variation in the parameters and allow us to analyse in more detail the behaviour of the asteroid in the presence of SRP.

In Figures 6.3 and 6.4 changes in the linear velocity and acceleration of the CoM of the asteroid are observed, it is seen how the small-body starts accelerating due to the effect of the SRP force. It is important to notice the differences in attitude by looking at the body-frame quaternion in Figure 6.5, when comparing both cases it is seen how the small-body starts rotating at a small rate over one orbit, as a result of the SRP torque and the irregular shape of the asteroid. It is also important to notice the periodic behaviour of the orbital elements of the asteroid in Figure 6.6 and we can see the perturbation in the semi-major axis in Figure 6.7 confirming that the shape of the orbit is changing over time. In Figures 6.9 and 6.10 the magnitude of the SRP force and torque acting on the asteroid is presented.

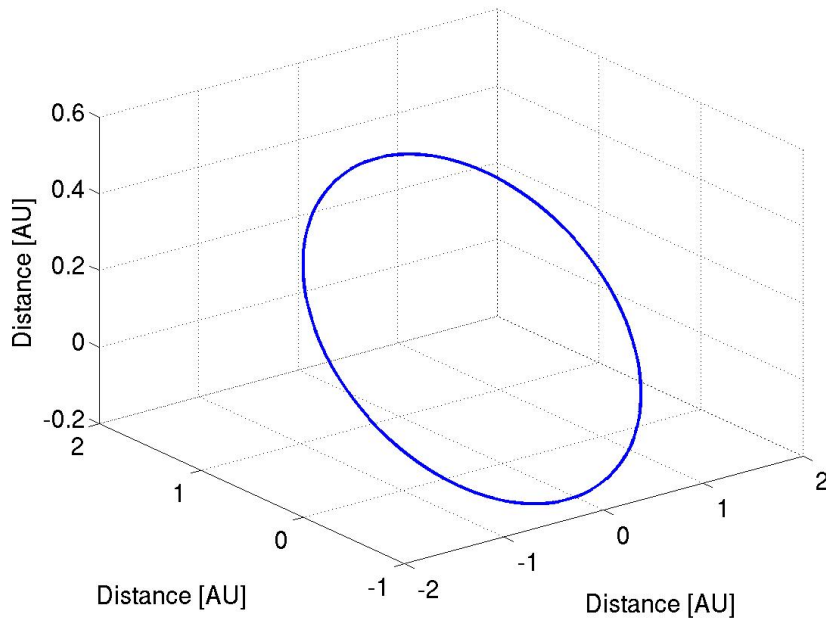
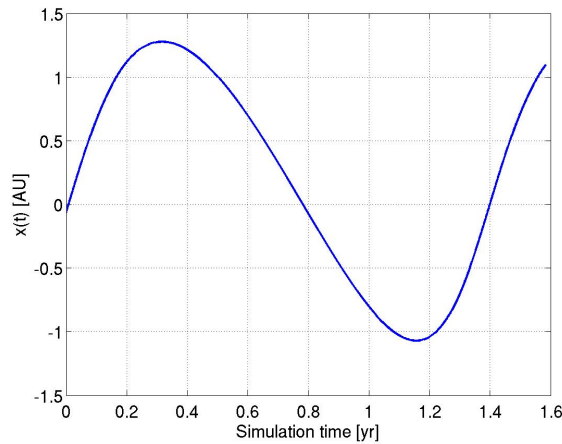


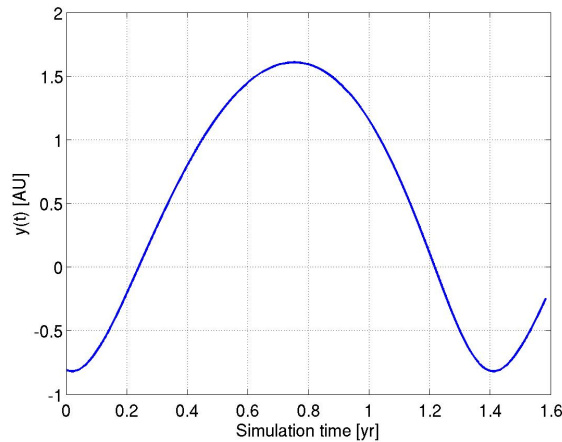
**Figure 6.1:** Orbital trajectory of the centre-of-mass of asteroid (1620) Geographos

---

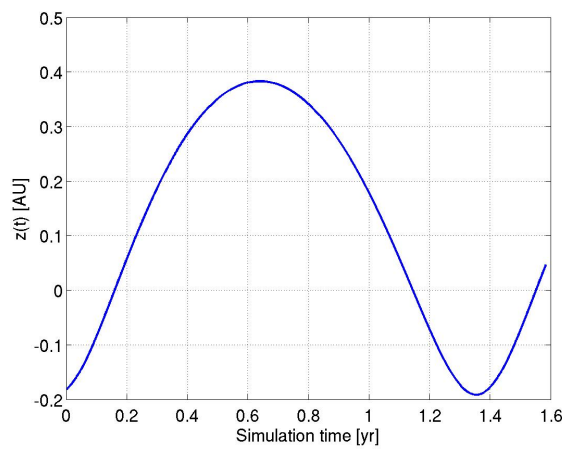
<sup>1</sup>True anomaly has been restricted between  $[0, \pi]$ , in reality is always an increasing angle.



(a) CoM position x-axis component



(b) CoM position y-axis component



(c) CoM position z-axis component

**Figure 6.2:** (1620) Geographos CoM Position [AU] vs Simulation Time [yr]

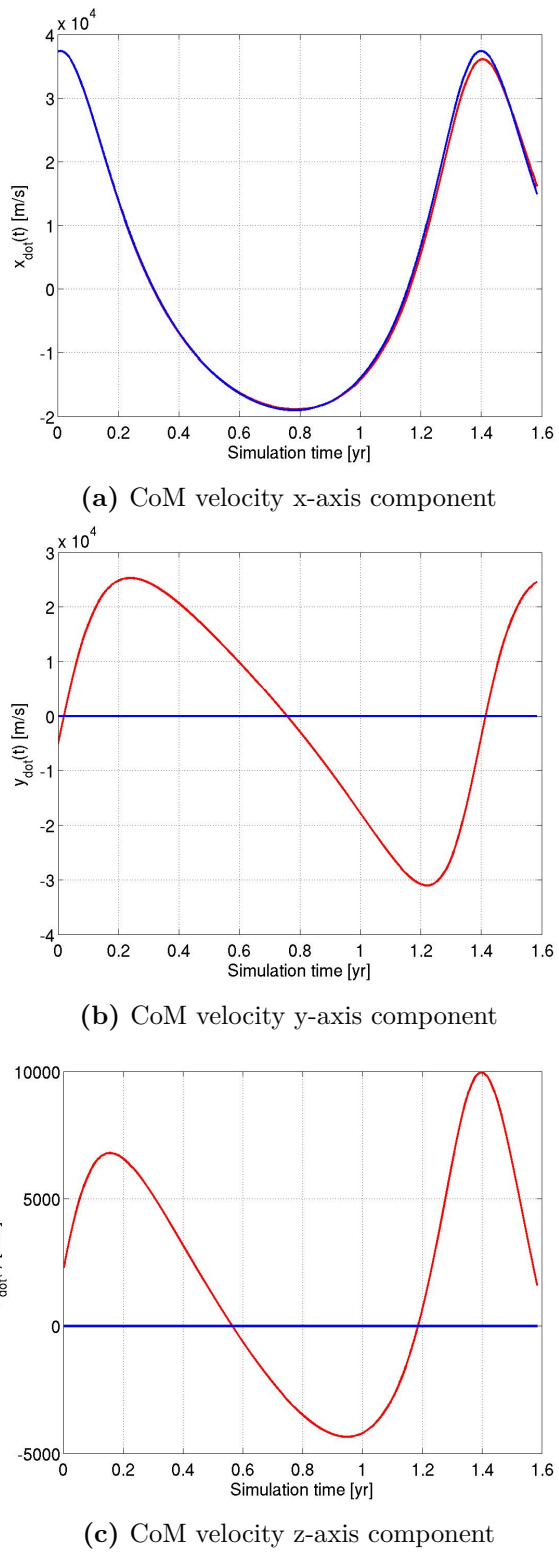
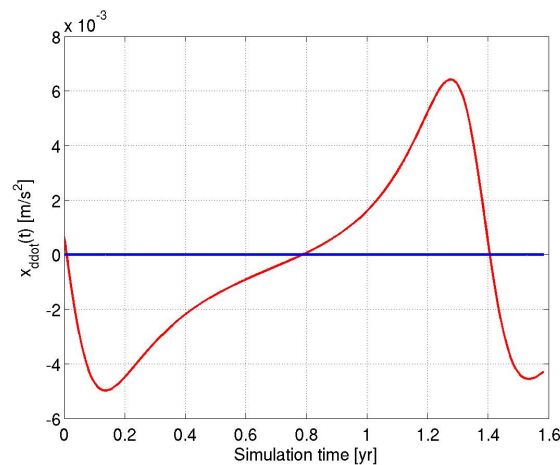
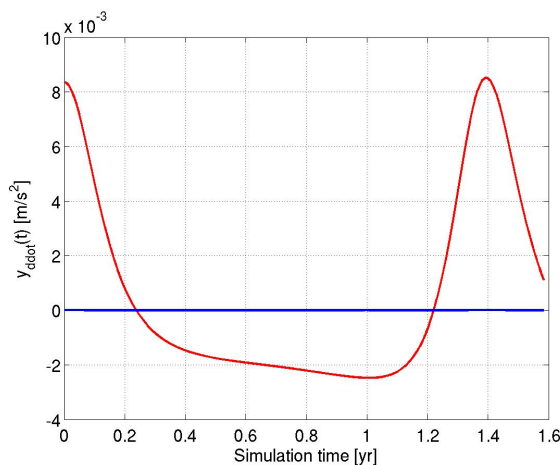


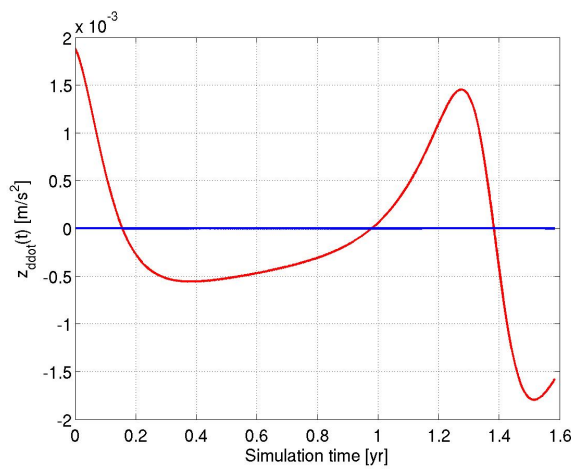
**Figure 6.3:** (1620) Geographos CoM Velocity  $\left[\frac{\text{m}}{\text{s}}\right]$  vs Simulation Time [yr]



(a) CoM acceleration x-axis component



(b) CoM acceleration y-axis component



(c) CoM acceleration z-axis component

**Figure 6.4:** (1620) Geographos CoM Acceleration  $\left[\frac{m}{s^2}\right]$  vs Simulation Time [yr]

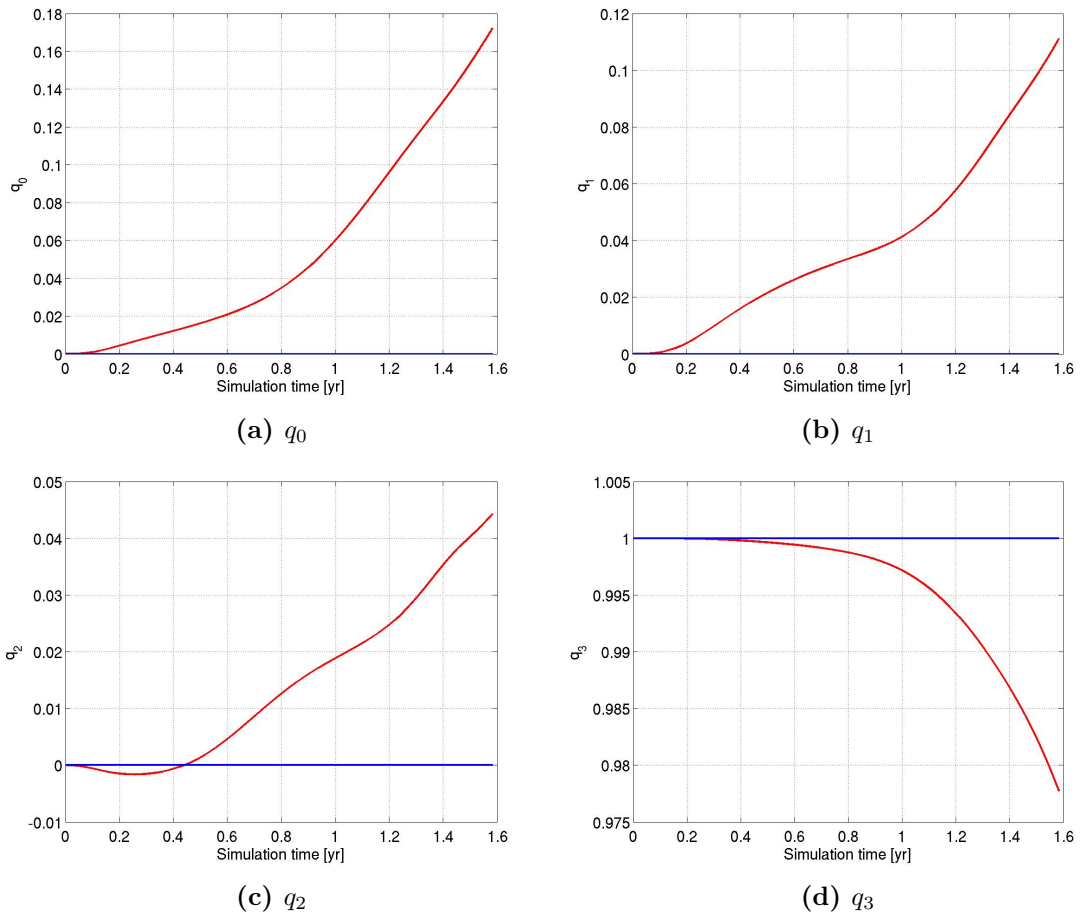
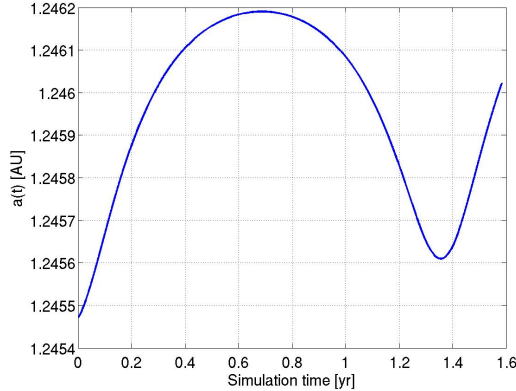
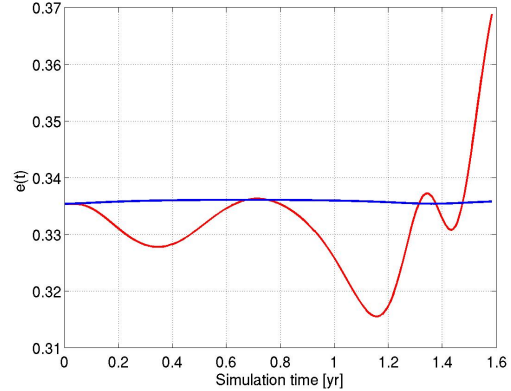


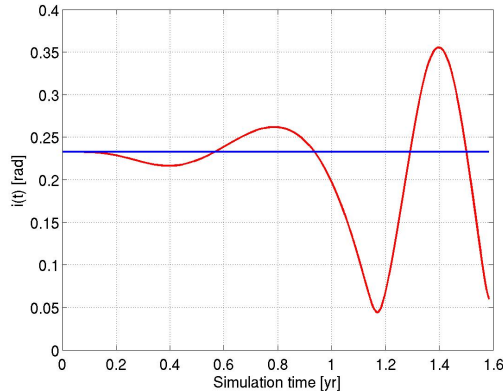
**Figure 6.5:** (1620) Geographos body-frame quaternion vs Simulation Time [yr]



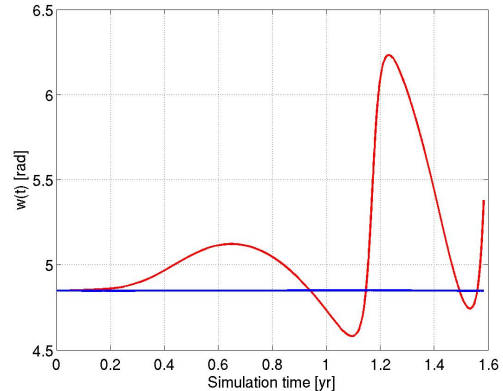
(a) Semi-major axis



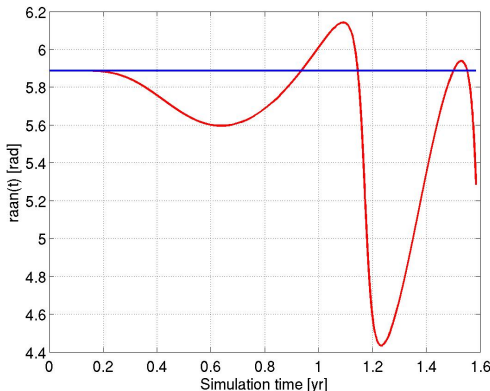
(b) Eccentricity



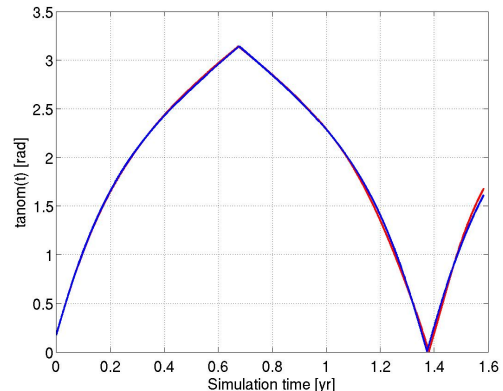
(c) Inclination



(d) Argument of the perihelion

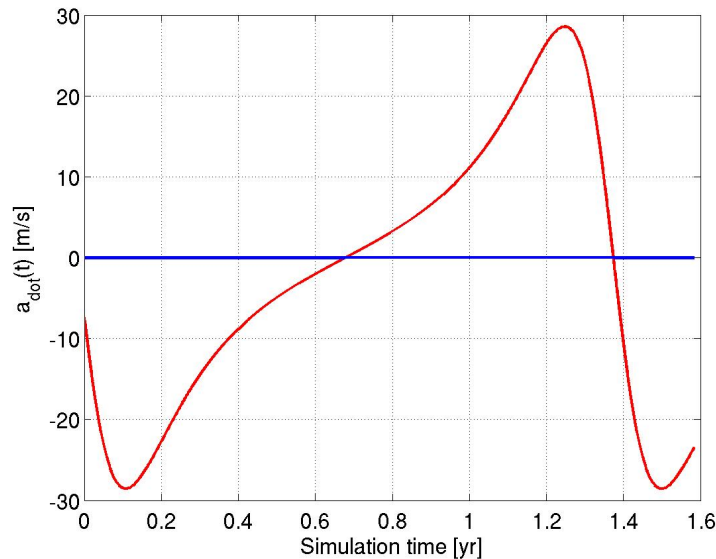


(e) Longitude of ascending node

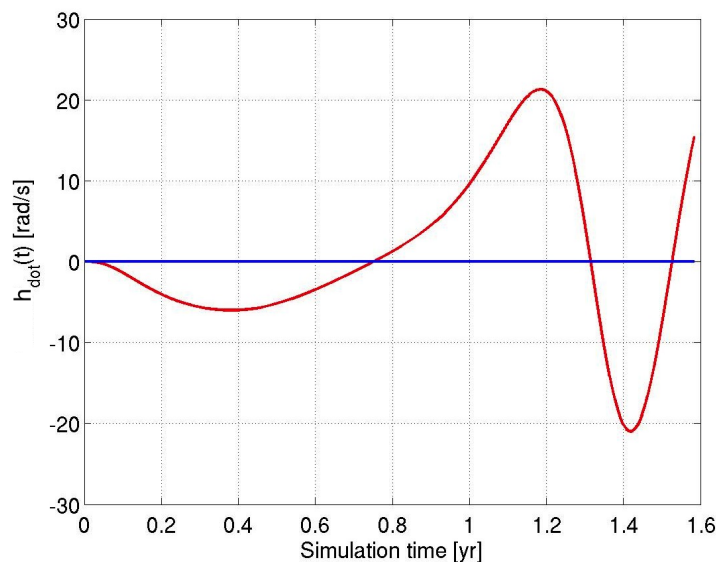


(f) True anomaly<sup>1</sup>

**Figure 6.6:** (1620) Geographos Orbital Elements vs Simulation Time [yr]

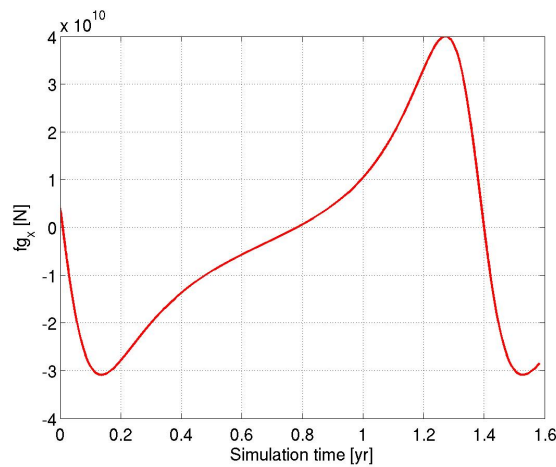


(a) Variation of semi-major axis

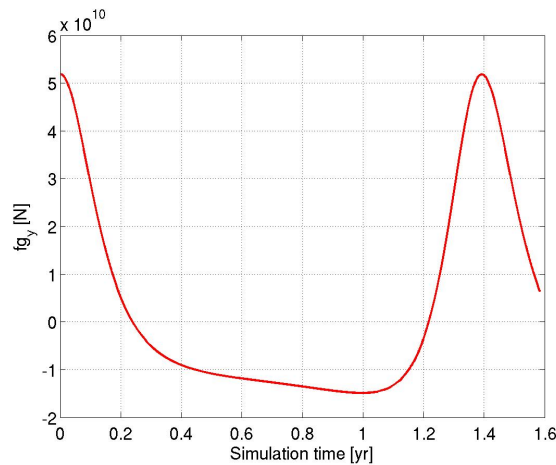


(b) Variation of the angular momentum

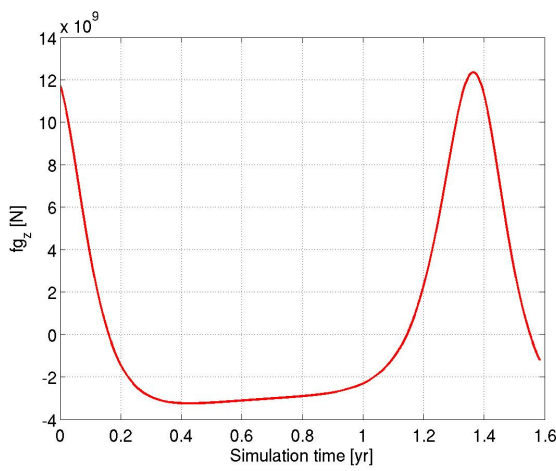
**Figure 6.7:** (1620) Geographos Perturbation in Orbital Elements vs Simulation Time [yr]



(a) Gravitational force x-axis component

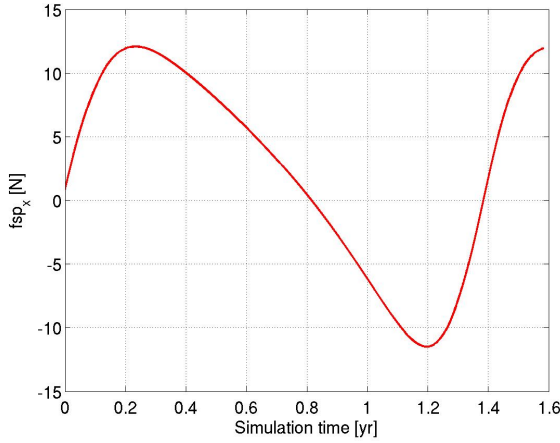


(b) Gravitational force y-axis component

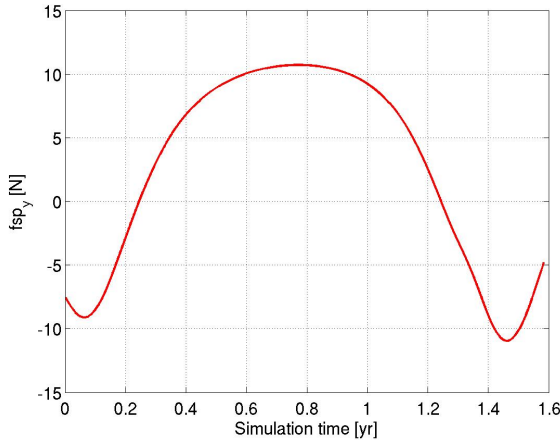


(c) Gravitational force z-axis component

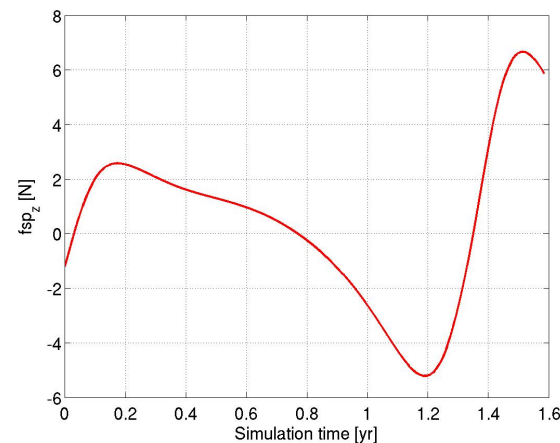
**Figure 6.8:** (1620) Geographos Gravitational Force [N] vs Simulation Time [yr]



(a) SRP force x-axis component

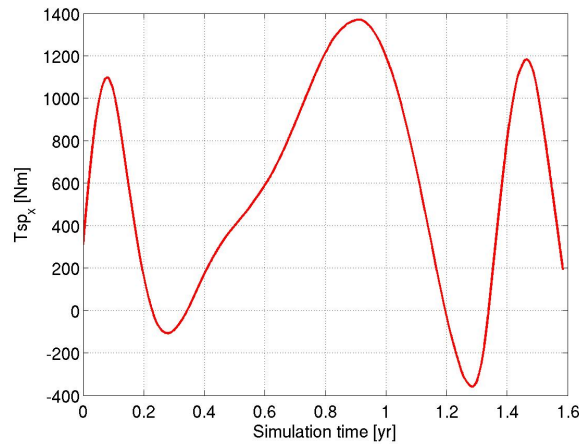


(b) SRP force y-axis component

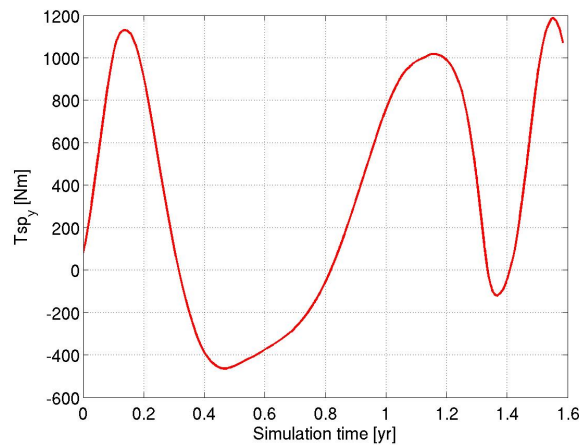


(c) SRP force z-axis component

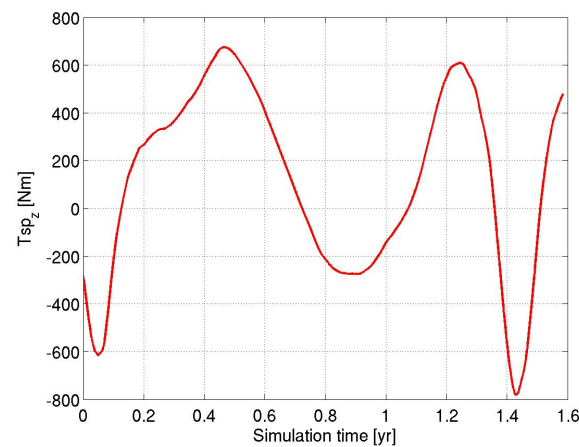
**Figure 6.9:** (1620) Geographos SRP Force [N] vs Simulation Time [yr]



(a) SRP torque x-axis component



(b) SRP torque y-axis component



(c) SRP torque z-axis component

**Figure 6.10:** (1620) Geographos SRP Torque [Nm] vs Simulation Time [yr]

## 6.2 Thin Solar Sail

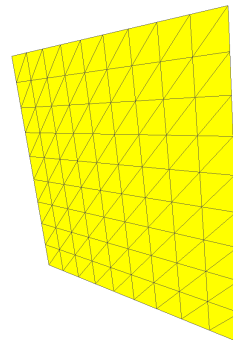


**Figure 6.11:** Solar sail Finite Element Model

For this test a squared solar sail is modelled in a fixed position in space, then modifying the incident angle is possible to get a validation case for our model. The following parameters have been used:

$$\tilde{r} = 1, s = 1, B_f = \frac{2}{3}, B_b = \frac{2}{3}, \varepsilon_f = 0, \varepsilon_b = 0$$

Transforming these parameters to the ones found in the P.C. Hughes Model [10] using Equations 3.18, 3.19, 3.20 and 3.21 we obtain:

$$\sigma_{rs} = 1, \sigma_{rd} = 0, \sigma_a = 0$$

Now we proceed to validate our SRP force model in Python[26] by comparing it to the results found in [14] for a square solar sail with a total area of  $100 \times 100 m^2$  and fixed located at 1 AU. This is done by calculating the SRP force for a range of incident angles between 0 and 90 degrees. Two test cases were developed, the first of them test the SRP Force model found in [25], the solar sail is modelled as a rigid body, a single area of  $10000 m^2$ . For the second case the Finite Area Elements Model (FEM) is tested, using a MATLAB script it was possible to create a Solar Sail of the same area as the previous case but divided in finite elements of area, as can be seen in Figure 6.11, a .obj file with 100 Vertices and 162 Facets was created to perform the test of the SRP model found in [10]. Using DataThief (<http://www.datathief.org/>) it was possible to extract the data for an ideal sail found in [14], a figure comparing the results thrown by our SRP Force models and the ideal sail is presented.

In Figure 6.12 it is possible to observe the similarity of the curves, our Python[26] models prove to be valid and provide similar results to those found in [14] for an "ideal sail", moreover as can be seen in Figure 6.13(a) the error between the SRP force exerted by the single area and the area divided in finite elements is almost null, which also demonstrates the correctness of our finite element SRP model. On the other hand as seen in Figure 6.13(b) the error between the ideal sail found in [14] and the force exerted by our FEM model is small.

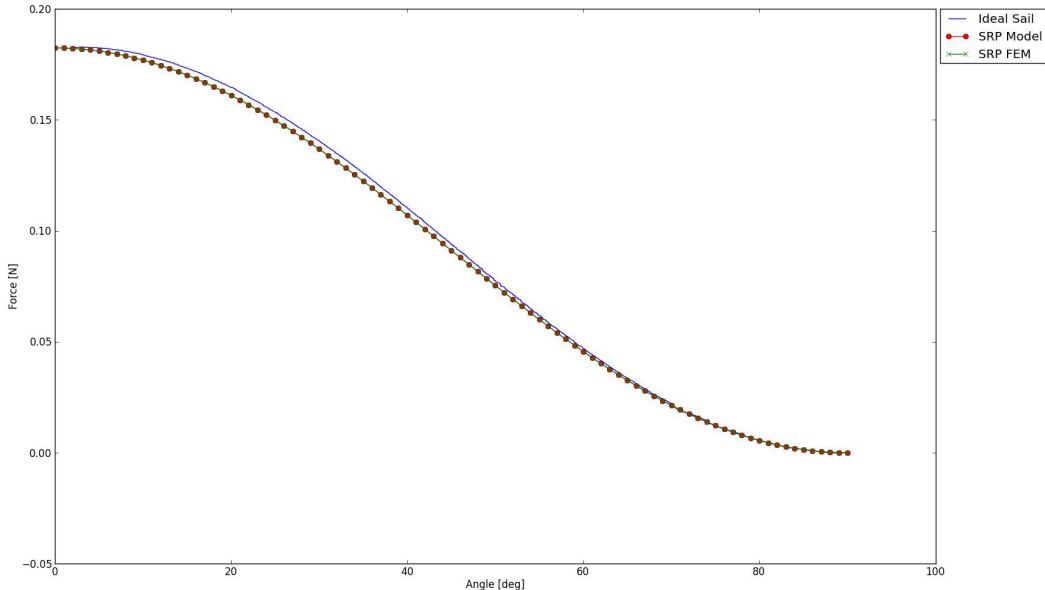
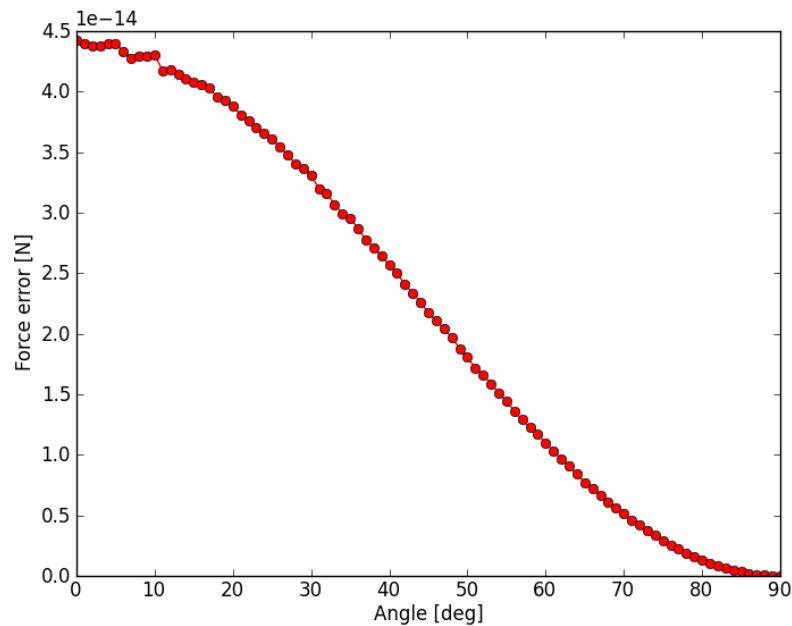
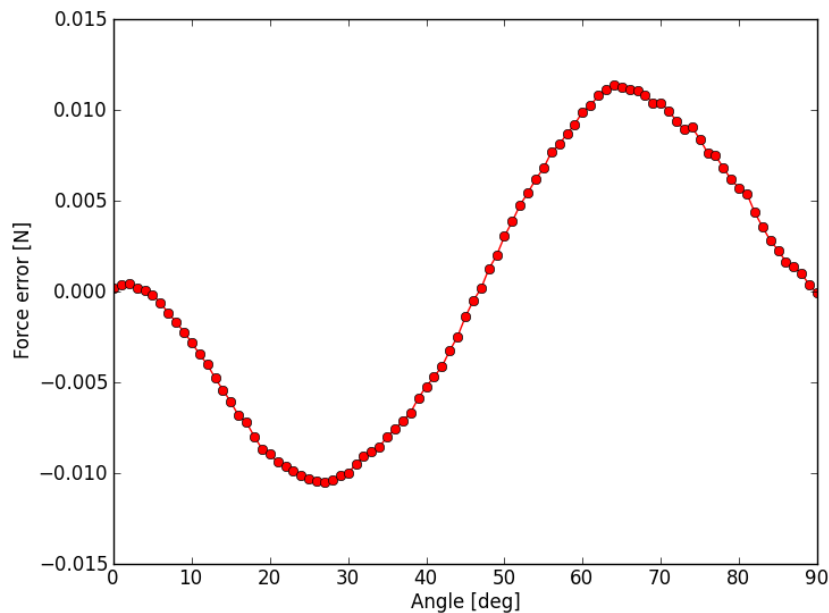


**Figure 6.12:** Force exerted on a  $100 \times 100 \text{ m}^2$  square solar sail at 1 AU



(a) Force Error between the SRP single area model and SRP FEM



(b) Force Error between the SRP Force exerted by an Ideal Sail and FEM Model of the Sail

**Figure 6.13:** Force Error [N] vs Incident Angle [deg]

## 6.3 Shadowing Effects

### 6.3.1 Theoretical Method

When studying the SRP acting on an asteroid and in our particular case when determining the facets that are illuminated by the Sun rays, it is important to take into account the possible Shadowing effects on the asteroid. The illumination geometry is defined by the unit vectors from the asteroid toward the Sun and the observer [27]. The sunlight is modelled as a collection of rays that allow us to determine the Shadowing effects in the body that may occur in two ways, the first being the self-shadowing effect, it appears due to the shape of the asteroid making so that some facets "block" the Sun rays and generate shadowing regions in areas that normally, because of the incident angle, would be considered as illuminated by our SRP Model. The second case occurs when other celestial or non celestial bodies enter the path of the light creating shadows in the asteroid and changing the orbital dynamics.

### 6.3.2 Implementation

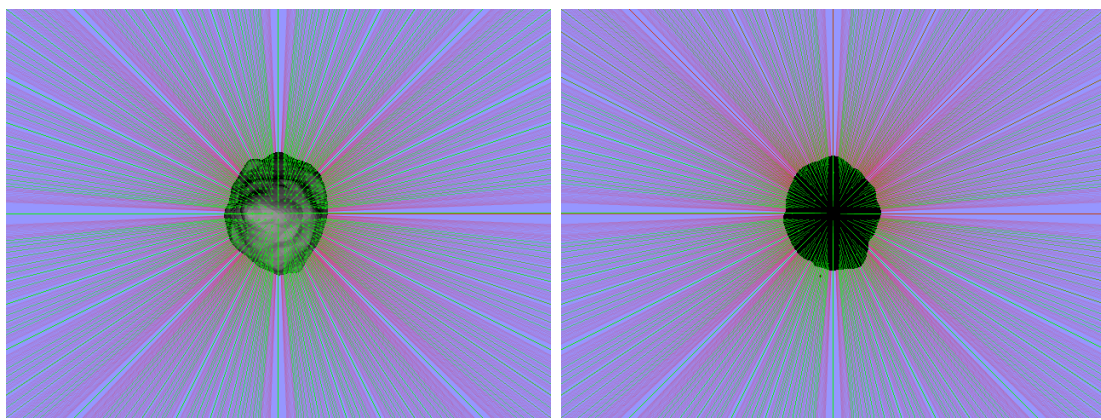


**Figure 6.14:** Render showing the ray grid collision test

The illumination geometry is implemented by modelling the Sun rays with a Ray-Tracing algorithm employing a ray collision test that integrates the rayTest function and Collision Detection capabilities of Bullet Physics [6] and the possibility of modelling rigid bodies of different nature, such as primitive objects and polyhedral meshes.

In Figure 6.14 the ray collision test is displayed, it consist of a grid of rays, in

which the initial position is the position of the Sun and the final position is a point located at the other side of the body. The number of rays can be changed depending on the precision needed, although the distance between rays should be small enough to cover all the facets in the surface of the body. The rays that collide with the body are displayed in green, while the ones that do not collide are displayed in red, also a green sphere is added at every position where a collision is detected. Render in Figure 6.14a shows the asteroid from the Sun in a front perspective, render in Figure 6.14b shows it from a point behind the asteroid towards the sun allowing us to observe the collisions in the "shadowed" areas.

### 6.3.3 Shadowing Function

The capability of tracking the position of the collisions in the surface of the body allow us to implement an algorithm that "Illuminates" the facets that contain at least one collision position. Since with the rayCollisionTest it is not possible to modify the colour of single facets in the .obj file, a different approach is taken, performing an emission gradient around each collision detected. The gradient consist of a circular area with a defined radius of action, which is selected to be approximately within the range of the size of the facets. As can be seen in Figure 6.15, adding the gradients of all the detected collisions give us a display of the areas illuminated and shadowed by the sunlight. Figure 6.15a, 6.15b, 6.15c and 6.15d show from different perspectives the results of the test perform on asteroid (1620) Geographos including the shadowing function.

In Figure 6.16 the results from the test performed on a sphere are displayed. As a main difference with the asteroid mesh, this primitive object does not have any collisions in regions that are in shadows, all the rays stay in the illuminated side and none of them pierce through the body reaching the other side.

In Figure 6.17 the results from the test performed on our Solar Sail FEM mesh (.obj) is shown. In this particular test a problem with the Bullet [6] object occurred: the Bullet[6] object that detects collision created after making the transformation from the .obj object results to be larger than the original, this is why collisions outside of the area of the sail are detected because there is a separation between the physical object in which the shadowing function takes place and the Bullet[6] object that is used solely to perform the collision detection. Nevertheless as can be seen the area facing the Sun is illuminated by our shadowing function.

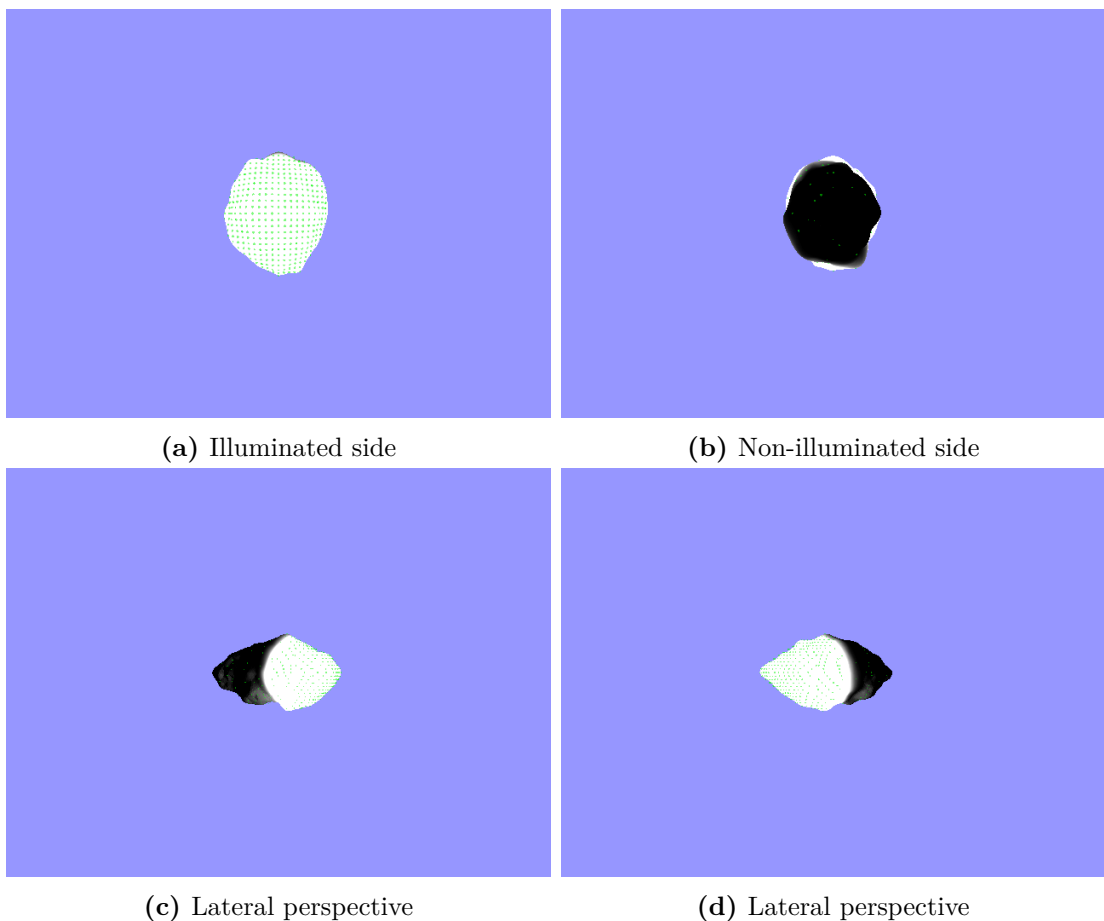


**Figure 6.15:** Render showing the shadowing function on asteroid (1620) Geographos

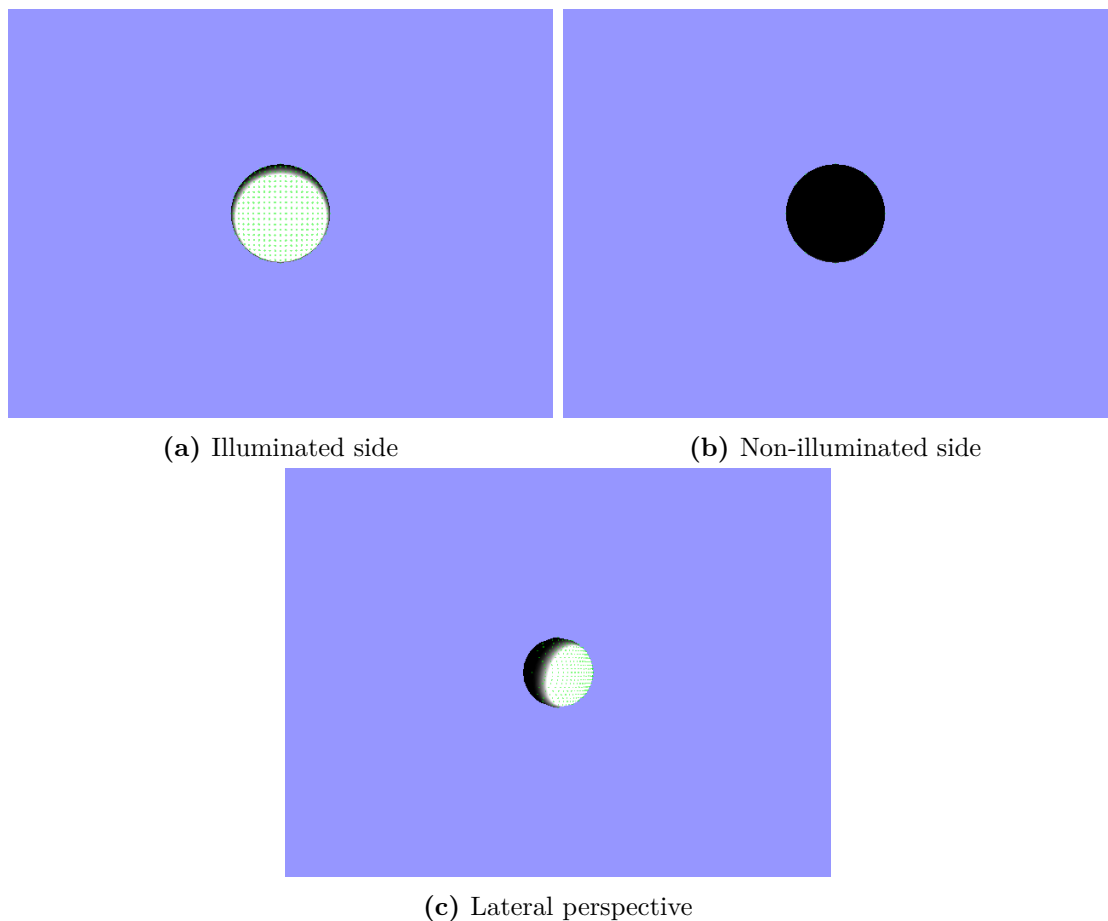


**Figure 6.16:** Render showing the shadowing function on a primitive object (Sphere)

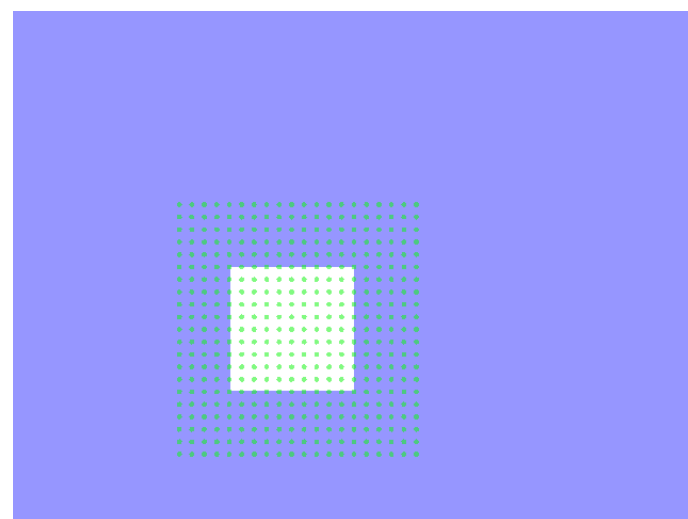


**Figure 6.17:** Illuminated solar sail with collision points



# Chapter 7

## Conclusions and Future Work

The aim of this research was to study the main external perturbations that influence the dynamics of Near Earth Asteroids (NEA) and implement their models into the DSENDSEduSims platform. In the environment of interest, the forces and torques generated by the Solar Radiation Pressure (SRP) and the gravitational potential of Earth and Moon (Planetary Gravity) are considered as the primary disturbance sources.

The *first contribution* of this thesis was finding an appropriate model for SRP, that can be applied to the irregular shape of an asteroid, in order to create a Python[26] function that feeds up the global simulation. Three different models were explored. The first one was the model of SRP for a rigid body, the second one was the model of SRP for a body with finite elements of area and the third one was the model of SRP for a solar sail. The rigid body model was the starting point to study how the incoming light is specularly reflected, diffusely reflected or absorbed. It turned out to be inappropriate because of the lack of consideration of the variation in the cross-sectional area exposed to the sun. For the second model, as a contrast with the former, the variation of the total area exposed to the Sun was measured. This was accomplished by dividing the surface of the asteroid into finite elements of area and subsequently adding the areas that were exposed to the Sun. This model was used during the simulation of the orbital dynamics and attitude of the asteroid. The solar sail model had a similar structure to the prior and it was used to validate the correctness of the implemented Python[26] functions, by comparing the results of the computed SRP force with those found in trusted bibliography for the specific case of a solar sail.

The *second contribution* was made by means of a simulation test of the dynamics of asteroid (1620) Geographos was performed for the free response and forced response of the system. A convenient polyhedron-shaped model of the asteroid, composed by triangular facets of small area, was established. When comparing the results of both cases, the following conclusion can be drawn that the variation of

the semi-major axis and true anomaly, due to the effect of SRP, over an orbit was little. However, significant changes in the state vector and attitude of the body were observed, in addition to an important drift in the rest of the orbital elements. Leading to the conclusion that it is the cumulative effect over sufficiently long periods of time that introduce a substantial change in the orbital dynamics of the asteroid. Meaningful changes in the body frame quaternion were identified, confirming that due to the irregular shape of the asteroid, the SRP generates a torque that makes the asteroid spin and therefore changes its attitude.

The *third contribution* of the research was modelling the shadow effects that appear as a result of the irregular shape of the small-body or the partial block of the sunlight by another body.

The *fourth contribution* was modelling and developing a Python[26] routine to compute the gravitational potential and gravitational acceleration of Planets using spherical harmonics. Specific cases for Earth and Moon were further studied. Even if a simulation of the asteroids' dynamics including the gravitational force of the aforementioned bodies was not performed, the perturbing force caused by higher degree and order of spherical harmonics is worth to be taken into consideration depending on the specific precision required in the overall study.

To conclude, future work is suggested. First, the simulation of the dynamics of the asteroid over a greater number of orbits would help to give more information of the steady state behaviour of the system. Second, it is recommended to perform multiple test cases for different NEA, in contemplation of a more complete assessment of the effect of the external perturbations in the orbital dynamics and attitude of small-bodies. Third, state a precision range that is desired on the base of the Gauss equations for the variation of the orbital elements. Last but not least, include the Yarkovsky-O'Keefe-Radzievskii-Paddack (YORP) effect as a main perturbation in the case of binary asteroids, since the difference in their composition and the not evenly re-emitted heat, contribute to larger generated torques and for this reason more significant changes in the attitude.

# Appendix A

## Quaternion definitions

### A.1 Quaternion representation

The representation of relative orientation using Euler angles is easy to develop and to visualize, but computationally intense. Also a singularity problem (Gimbal lock) occurs when describing attitude kinematics in terms of Euler angles and therefore it is not an effective method for asteroid attitude dynamics. The widely used quaternion representation is based on Euler's rotational theorem which states that the relative orientation of two coordinate systems can be described by only one rotation about a fixed axis[8]. A quaternion is a  $4 \times 1$  matrix which elements consists of a vector part  $\underline{q}_v$  and a scalar part  $q_s$ . As follows:

$$\underline{q} = \begin{bmatrix} \underline{q}_v \\ q_s \end{bmatrix} \quad (\text{A.1})$$

The vector part in  $\underline{q}_v$  of Equation A.1 might be expressed in a cartesian coordinate system as:

$$\underline{q}_v = q_0 \hat{i} + q_1 \hat{j} + q_2 \hat{k} \quad (\text{A.2})$$

Where the unit vectors  $\hat{i}$ ,  $\hat{j}$  and  $\hat{k}$  are defined as:

$$\hat{i} = \begin{bmatrix} 1 \\ 0 \\ 0 \end{bmatrix}, \quad \hat{j} = \begin{bmatrix} 0 \\ 1 \\ 0 \end{bmatrix}, \quad \hat{k} = \begin{bmatrix} 0 \\ 0 \\ 1 \end{bmatrix}$$

Therefore using the vector part definition in Equation A.2 and using same notation for the scalar part, the quaternion in Equation A.1 changes into:

$$\underline{q} = \begin{bmatrix} q_0 \\ q_1 \\ q_2 \\ q_3 \end{bmatrix} \quad (\text{A.3})$$

## A.2 Quaternion math

The standard mathematical operation of quaternion are valid. In this appendix only the ones required for the attitude representation are introduced.

### A.2.1 Norm

The norm of the quaternion in Equation A.3 is defined as:

$$|\underline{q}| = \sqrt{q_0^2 + q_1^2 + q_2^2 + q_3^2}$$

A quaternion with norm  $|\underline{q}| = 1$  is a *unit quaternion*.

### A.2.2 Normalization

To transform a given quaternion to a unit quaternion it is divided by its norm, as follows:

$$||\underline{q}|| = \frac{\underline{q}}{|\underline{q}|}$$

### A.2.3 Conjugate

The conjugate of a quaternion is defined in the same way as Equation A.3 but with negative vector part, given as:

$$\underline{q} = \begin{bmatrix} -q_0 \\ -q_1 \\ -q_2 \\ q_3 \end{bmatrix} \quad (\text{A.4})$$

### A.2.4 Addition

Given two quaternions  $\underline{q}_1 = \begin{bmatrix} q_{v1} \\ q_{s1} \end{bmatrix}$  and  $\underline{q}_2 = \begin{bmatrix} q_{v2} \\ q_{s2} \end{bmatrix}$ , its addition  $\underline{q}$  is defined as:

$$\underline{q} = \underline{q}_1 + \underline{q}_2 = \begin{bmatrix} q_{s1} + q_{s2} \\ \underline{q}_{v1} + \underline{q}_{v2} \end{bmatrix}$$

### A.2.5 Multiplication

Given two quaternions  $\underline{q}_1 = \begin{bmatrix} q_{v1} \\ q_{s1} \end{bmatrix}$  and  $\underline{q}_2 = \begin{bmatrix} q_{v2} \\ q_{s2} \end{bmatrix}$ , its product  $\underline{q}$  is defined as:

$$\underline{q} = \underline{q}_1 \otimes \underline{q}_2 = \begin{bmatrix} q_{s1}q_{s2} - \underline{q}_{v1} \cdot \underline{q}_{v2} \\ q_{s1}\underline{q}_{v2} + q_{s2}\underline{q}_{v1} + \underline{q}_{v1} \times \underline{q}_{v2} \end{bmatrix}$$

Where  $\cdot$  is the dot product between the vectors and  $\times$  is their cross product.



# Bibliography

- [1] Osman Ersed Akcasu and Ibrahim Akcay. Solar timer using gps technology, October 31 2012. US Patent App. 13/665,465.
- [2] Justin A ATCHISON and Mason A PECK. Length scaling in spacecraft dynamics. *Journal of guidance, control, and dynamics*, 34(1):231–246, 2011.
- [3] KH Bhavnani and RP Vancour. Coordinate systems for space and geophysical applications. Technical report, DTIC Document, 1991.
- [4] William F Bottke Jr, David Vokrouhlický, David P Rubincam, and David Nesvorný. The yarkovsky and yorp effects: Implications for asteroid dynamics. *Annu. Rev. Earth Planet. Sci.*, 34:157–191, 2006.
- [5] David Capek. *Thermal Effects in Physics and Dynamics of Small Bodies of the Solar System*. PhD thesis, Charles University, Faculty of Mathematics and Physics Astronomical Institute, 2007.
- [6] E Coumans. Bullet physics library website. Available in: <http://www.bulletphysics.com>, 2007.
- [7] Robert G Gottlieb. Fast gravity, gravity partials, normalized gravity, gravity gradient torque and magnetic field: derivation, code and data. *Unknown*, 1, 1993.
- [8] K Großekathöfer and Z Yoon. Introduction into quaternions for spacecraft attitude representation. *TU Berlin*, 2012.
- [9] Simon A Holmes and Will E Featherstone. A unified approach to the clenshaw summation and the recursive computation of very high degree and order normalised associated legendre functions. *Journal of Geodesy*, 76(5):279–299, 2002.
- [10] Peter C Hughes. *Spacecraft attitude dynamics*. J. Wiley and Sons, 1986.

## BIBLIOGRAPHY

---

- [11] Lasunncety. Diagram illustrating and explaining various terms in relation to orbits of celestial bodies. Available in: <http://en.wikipedia.org/wiki/File:Orbit1.svg>, 2007.
- [12] James M Longuski, Richard E Todd, and Wolfgang W Koenig. Survey of nongravitational forces and space environmental torques-applied to the galileo. *Journal of guidance, control, and dynamics*, 15(3):545–553, 1992.
- [13] E Mazarico, FG Lemoine, Shin-Chan Han, and DE Smith. Glgm-3: A degree-150 lunar gravity model from the historical tracking data of nasa moon orbiters. *Journal of Geophysical Research: Planets (1991–2012)*, 115(E5), 2010.
- [14] Colin R McInnes. Solar sailing. *Solar Sailing, XXIX, 296 pp... Also Springer-Praxis Series*, 1, 1999.
- [15] Merriam-Webster. Archimedean spiral. Available in: [http://www.merriam-webster.com/dictionary/Archimedean spiral](http://www.merriam-webster.com/dictionary/Archimedean%20spiral), Mar 2014.
- [16] Oliver Montenbruck and Gill Eberhard. *Satellite orbits: models, methods, and applications*. Springer, 2000.
- [17] K Muinonen and JSV Lagerros. Inversion of shape statistics for small solar system bodies. *Astronomy and Astrophysics*, 333:753–761, 1998.
- [18] University of Waikato. Types of reflection. Available in: <http://www.sciencelearn.org.nz/Contexts/Light-and-Sight/Sci-Media/Images/Types-of-reflection>, 2012.
- [19] NK Pavlis, SA Holmes, SC Kenyon, and JK Factor. An earth gravitational model to degree 2160: Egm2008. presentation given at the 2008 european geosciences union general assembly held in vienna, austria, 13–18 apr 2008. Available in: <http://earth-info.nga.mil/GandG/wgs84/gravitymod/egm2008>, 2008.
- [20] Rod Pierce. "normal distribution" math is fun. Available in: <http://www.mathsisfun.com/data/standard-normal-distribution.html>, 2014.
- [21] Salvatore Santoli. Carbon nanotube membrane solar sails a challenge for extremely fast space flight. Available in: <http://www.intechopen.com/books/export/citation/BibTex/carbon-nanotubes/carbon-nanotube-membrane-solar-sails-a-challenge-for-extremely-fast-space-flight>, 2010.
- [22] Daniel J Scheeres. Orbital motion in strongly perturbed environments. *Orbital Motion in Strongly Perturbed Environments*, by Scheeres, Daniel J. ISBN: 978-3-642-03255-4. Berlin: Springer, 2012, 1, 2012.

---

## BIBLIOGRAPHY

---

- [23] EM Standish. Jpl planetary and lunar ephemerides, de405/le405//interoffice memorandum, 1998. 312. Technical report, F-98-048.
- [24] S.T. Suess and B.T. Tsurutani. Solar winds. *Encyclopedia of Atmospheric Sciences, Academic Press London*, pages 2078–2085, 2002.
- [25] D VALLADO. *Fundamentals of astrodynamics and applications*. Microcosm Press and Springer, 2007.
- [26] Guido Van Rossum et al. Python programming language. In *USENIX Annual Technical Conference*, 2007.
- [27] Olli Wilkman and Karri Muinonen. Asteroid lightcurve phase shift from rough-surface shadowing. *Meteoritics & Planetary Science*, 2013.
- [28] D Yeomans. Nasa/ jpl near-earth object program office statement, 2008.

